Improving Electrochemical Methods of Producing Hydrogen in Alkaline Media via Ammonia and Urea Electrolysis

A dissertation presented to

the faculty of

the Russ College of Engineering and Technology of Ohio University

In partial fulfillment

of the requirements for the degree

Doctor of Philosophy

Bryan Kenneth Boggs

March 2010

This dissertation titled

Improving Electrochemical Methods of Producing Hydrogen in Alkaline Media via Ammonia and Urea Electrolysis

by

Bryan Kenneth Boggs

has been approved for

the Department of Chemical and Biomolecular Engineering

and the Russ College of Engineering and Technology by

Gerardine G. Botte

Professor of Chemical and Biomolecular Engineering

Dennis Irwin

Dean, Russ College of Engineering and Technology

ABSTRACT

BOGGS, BRYAN KENNETH, Ph.D., March 2010, Chemical and Biomolecular Engineering.

Improving Electrochemical Methods of Producing Hydrogen in Alkaline Media via Ammonia and Urea Electrolysis (100 pp.)

Director of Dissertation: Gerardine G. Botte

Theoretically, ammonia electrolysis consumes 95% less energy than its major competitor water electrolysis and offers an economical, environmental, and efficient means for reducing nitrate contaminations in ground and drinking water. Thermodynamically at standard conditions, ammonia electrolysis consumes 1.55 Wh to produce one gram of hydrogen. This same gram of hydrogen generates 33 Wh utilizing a proton exchange membrane fuel cell (PEMFC). There is a potential of 31.45 Wh of net energy when coupling an ammonia electrolytic cell (AEC) and a PEMFC. Considering that PEMFCs are 60% efficient, the actual energy output ranges between 18 and 20 Wh. Prior to the research shown here, ammonia electrolysis in alkaline media was requiring more than 20 Wh of energy input due to slow anode kinetics and poor electrochemical cell design thus making any chances of a self-sustaining energy generator unfeasible. This research focused on improving and optimizing anode electrocatalyst materials, electrode configurations, and cell designs, as well as demonstrating stationary and mobile applications of ammonia electrolysis.

In addition to ammonia electrolysis, a novel electrochemical technique, urea electrolysis in alkaline media, was created and investigated. Similar to ammonia

electrolysis, the anodic reaction, which is the oxidation of urea, was found to be the most rate-limiting half-cell reaction and required improvement. This research focused on fundamentally understanding the mechanism of urea electrolysis as well as investigating common electrocatalysts for small organic molecules. As a result, urea electrolysis in alkaline media proved to be a direct, economical, and environmental approach to producing hydrogen electrochemically with an inexpensive transition metal.

Approved: _____

Gerardine G. Botte

Professor of Chemical and Biomolecular Engineering

ACKNOWLEDGMENTS

There are several people who made a significant impact on my life over the past few years that I would like to acknowledge. Without their emotional and physical support, conquering such an immense task such as this degree would have been unconquerable. First and foremost, I would like to thank my parents for all that they have given me since my conception. It is because of their resilience, dedication, and support that I aspired to be a successful scientist and human. Second and just as important, I would like to demonstrate my gratitude in appreciation for Dr. Gerardine G. Botte. Her willingness, commitment, encouragement, and foresight allowed me to see my own potential for which I will be forever indebted to. Third, I would like to thank my best friend, comrade, and protégé, Becky King. Words alone cannot describe what she has done for me in recent years so suffice it to say "I Love You". Lastly, I wish to thank my committee members Dr. Howard Dewald, Dr. Valerie Young, Dr. Daniel Gulino, and Dr. Saw-Wai Hla for both their guidance and direction.

TABLE OF CONTENTS

Page

LIST OF TABLES

LIST OF FIGURES

CHAPTER 1. INTRODUCTION

1.1 Project Overview

Today, fuel cells are increasing in popularity as alternative energy suppliers. Fuel cells, in particular, proton exchange membrane (PEM) produce clean water that is exhausted to the atmosphere quietly with 60% efficiency; however, major problems still exist. Storing and producing hydrogen are still serious tribulations that are delaying the commercialization and marketplace acceptance of fuel cells. Additionally, the cost of hydrogen is relatively high and offers no advantage over conventional gasoline. A study in Italy shows that hydrogen-operated vehicles, which utilize untaxed hydrogen, pay a little more at the pump than untaxed gasoline and diesel consumers. However, the health costs in Milan, Italy are expected to decrease by nearly $2 million per year [1].

Interest in hydrogen fuel-cell vehicles (HFCVs) has been increasing in popularity over the past decade. This is primarily a result of the shrinking oil reserves which are expected to last only 42 years as of 1998 [2]. HFCVs have also found a niche in the environmental and political fields because the scientific community is beginning to acknowledge the threat posed by harmful air pollutants such as nitrogen oxides (NO_x), volatile organic compounds (VOCs), carbon monoxide (CO), and sulfur dioxide (SO_2) caused by hydrocarbon-dependent vehicles [3-5]. In addition to being environmentally friendly, HFCVs are quiet and convert 50-60% of the energy available in hydrogen to power the automobile rather than the mediocre 20-30% efficiency of today's internal combustion engines [6, 7].

A hydrogen future is not only driven by the transportation sector but as a movement for reducing oil imports in general and eliminating the dependence on petroleum for daily energy production. By 2020, the world population is expected to increase from 6 to 7.4 billion. Understandably, the energy demand is expected to increase from 100.7×10^{12} to 160×10^{12} kW-h [2, 8]. For a hydrogen economy to evolve in our lifetime, hydrogen will need to be produced, distributed, and stored on a mass scale in a manner that is cost effective, environmentally advantageous, and efficient [9].

At the moment, there are issues with all three of these idealistic goals. Going back to HFCVs, producing hydrogen that is cost competitive with gasoline is proving to be difficult. Compared to gasoline, hydrogen has 2.7 times more energy content based on weight. Due to its tremendously low density, hydrogen has 25% less energy content than gasoline when based on volume [10]. Because of this, there is no storage technology currently available that allows a vehicle to travel the average 300-mile range that today's internal combustion engines obtain [11].

In an effort to accelerate hydrogen research and an attempt to surpass the problems associated with storage, President Bush pledged $1.2 billion in 2003. As a result, the U.S. Department of Energy (DOE) has established a legal-binding partnership with the U.S. Council on Automotive Research consisting of major U.S. automotive and energy companies called the FreedomCAR and Fuel Partnership which looks at the benefits of producing hydrogen on board [11]. This indicates a movement of refocusing attention on in situ hydrogen generating technologies.

These issues are a concern, and it is proposed to address both of these problems with one solution. That is, the use of either in-situ electro-oxidation of ammonia designed for on-board hydrogen production for fuel cell utilization or urea electrolysis for a more stationary application. This dissertation covers both the understanding and improvements of ammonia and urea electrolysis in alkaline media.

Producing hydrogen in-situ, or on board, is a solution for hydrogen storage problems. Hydrogen will be produced on demand and storing hydrogen will be deemed *unnecessary*. With respect to the high cost of hydrogen, both ammonia and urea electrolysis theoretically require less energy compared to current methods of mass hydrogen production. It's an undeniable fact that the need for improvement is a never-ending objective. Ammonia electrolysis has already been proven a successful means for hydrogen production. Ammonia has the potential to be a practical hydrogen-carrier fuel; it is a liquid fuel that can be stored at ambient temperature and pressure and is hydrogen dense and non-carbon containing [12]. Nevertheless, electrodes used to electrolyze aqueous ammonia (combination of potassium hydroxide KOH and ammonium hydroxide NH_4OH) are the heart of the process and can use improvement.

It was proposed to address the surface area of the electrodes while maintaining high electrical conductivity and low electrical resistance. In order to increase the surface area of the electrode's catalyst support, it was decided to use manufactured polyacrylonitrile (PAN) based carbon fiber paper (CFP). After 16 months of researching and experimenting several methods for electrode improvement including: electrically conductive pastes, Carbon Nanofibers (CNF), Chemical Vapor Deposition (CVD), and a

multitude of different ways to construct electrodes (160+ electrodes and 7 methods to be exact), the conclusion to use CFP as a catalyst support, for the replacement of carbon-fiber wrapped electrodes currently used in the lab, has been made.

It has been found through meticulous testing that Toray™ TGP-H-030 CFP offers all the characteristics desired for preparing reproducible electrodes. Those characteristics are: infinitesimal amount of unconductive polytetrafluoroethylene (PTFE) for hydrophobicity and fiber binding, high visual surface area, 80% porosity, and great electroplating capabilities.

1.2 Objectives

Presently, the cost of hydrogen provides no benefits over gasoline. This coupled with high pressures required for on-board hydrogen storage are the main reasons why fuel cell commercialization has been slow. It was determined through a series of calculations that ammonia electrolysis requires 95% less energy theoretically compared to its rival water electrolysis [12]. This has strong implications: lowers the production costs of hydrogen, allows batteries, solar, and wind power to provide the energy for electrolysis, enabling a hydrogen economy to evolve in our lifetime.

Theoretically, ammonia electrolysis requires 1.55 Wh g^{-1} H_2. For this same gram of H_2, a PEMFC generates 33 Wh suggesting that a net power is feasible. In the real world, fuel cells are typically 50-60% efficient, and the oxidation of ammonia has large overpotentials threatening the possibility of net energy.

Preceding carbon-fiber wrapped electrodes used in the lab were not scalable and had a tendency to deteriorate after testing. In addition, the power consumption of ammonia electrolysis was higher than the energy generated by a PEMFC. There is a 440 mV overpotential versus Hg/HgO for the anodic oxidation of ammonia. Because of this large overpotential, seven different methods for electrode preparation were analyzed. In the end, Toray TGP-H-030 carbon fiber paper (CFP) supported with titanium foil was chosen as the catalyst support because it offered great scalability and low energy consumption for the electrolysis of ammonia.

In addition to ammonia electrolysis, a new novel approach for directly converting urine-rich waste water into hydrogen was conceived and developed. Rather than converting urea into ammonia from municipal waste waters then electrolyzing it, urea electrolysis in alkaline media provided a method for directly evolving hydrogen while simultaneously remediating nitrate contamination. Within the context of these two distinctly different technologies, three general project objectives were created:

1. Improve the electro-oxidation of ammonia by way of catalyst optimization and electrode design (Chapter 2).
2. Determine the feasibility of using ammonia electrolysis as an on-board hydrogen storage and production technology (Chapter 3).
3. Understand the electrokinetics of urea electrolysis for proposing a reaction mechanism as well as choosing which catalyst is best suited for the rate-limiting oxidation reaction (Chapter 4).

For the first objective, several common catalysts in mono, bi, and ternary alloy form were investigated as potential catalysts. Pt-Ir alloy demonstrated to be the most active catalyst for ammonia oxidation in alkaline media and was investigated further. Optimizing key performance indicators such as maximizing the oxidation exchange current density and minimizing the oxidation overpotential was accomplished using a design of experiments that altered concentrations of Pt (IV) and Ir (III) in the electroplating bath as well as the total catalytic loading.

The second objective was to integrate an ammonia electrolytic cell with a breathable proton exchange membrane fuel cell so that energy consumption and production rates, respectively, could be determined. This quantifiable investigation allowed for comparison of ammonia as a hydrogen storage technology to the Department of Energy's 2010 strategic on-board hydrogen storage targets.

The third and final objective was to propose a reaction mechanism for urea electrolysis in alkaline media as well as investigate common electrocatalysts for oxidizing small organic compounds

1.3 References

1. R. Mercuri, A. Bauen and D. Hart, *Journal of Power Sources,* **106** (2002).
2. K. Weissermel and H. J. Arpe, *Industrial Organic Chemistry*, Wiley-VCH, Weinheim, Germany, **2003**.
3. M. Z. Jacobson, W. G. Colella and D. M. Golden, *Science,* **308** (2005).
4. M. Granovskii, I. Dincer and M. A. Rosen, *Journal of Power Sources,* **157** (2006)**.**
5. M. Granovskii, I. Dincer and M. A. Rosen, *Journal of Power Sources,* **167** (2007).
6. M. W. Melaina, *International Journal of Hydrogen Energy,* **28** (2003).
7. J. J. Hwang, D. Y. Wang and N. C. Shih, *Journal of Power Sources*, **141** (2005).
8. T. Beardsley, *Scientific American*, **271** (1994).
9. J. A. Turner, *The Electrochemical Society Interface,* 23 (2004).
10. M. Balat and N. Ozdemir, *Energy Sources*, **27** (2005).
11. S. Satyapal, J. Petrovic, C. Read, G. Thomas and G. Ordaz, *Catalysis Today*, **120** (2007).
12. F. Vitse, M. Cooper and G. G. Botte, *Journal of Power Sources*, **142** (2005).

CHAPTER 2.

OPTIMIZATION OF PT-IR ON CARBON FIBER PAPER FOR THE ELECTRO-OXIDATION OF AMMONIA IN ALKALINE MEDIA

It should be noted that part of the contents of this chapter have been submitted to a peer-reviewed journal for publication.

2.1 Abstract

Plating bath concentrations of Pt (IV) and Ir (III) have been optimized as well as the total catalytic loading of bimetallic Pt-Ir alloy for the electro-oxidation of ammonia in alkaline media at standard conditions. This was accomplished using cyclic voltammetry, scanning electron microscopy (SEM), energy dispersive X-ray (EDX), and statistical optimization tools. Concentrations of Pt (IV) and Ir (III) of the plating bath strongly influence electrode surface atomic compositions of the Pt-Ir alloy directly affecting the electro-oxidation behavior of ammonia. Several anode materials were studied using cyclic voltammetry, which demonstrated that Pt-Ir was the most active catalyst of those tested for the electro-oxidation of ammonia. Criteria for optimization were minimizing the climatic oxidation overpotential for ammonia and maximizing the exchange current density. Optimized bath composition was found to be 8.844 ± 0.001 g L^{-1} Pt (IV) and 4.112 ± 0.001 g L^{-1} Ir (III) based on electrochemical techniques. Physical characterization of the electrodes by SEM indicates that the plating bath concentrations of Pt and Ir influence the growth and deposition behavior of the alloy.

2.2 Introduction:

2.2.1 Ammonia electrolysis

Aqueous ammonia's high capacity for hydrogen storage has led to increased interest in using ammonia as an alternative energy carrier [1,2]. Extracting this hydrogen from ammonia can be accomplished through the use of a novel electrochemical approach. According to Vitse *et al*. [3,4], ammonia electrolysis consumes 95% less energy than water electrolysis theoretically at standard conditions and produces hydrogen at a cost of \$0.89 per kg, which is significantly less than the \$2-3.00 kg^{-1} goal set forth by the U.S. Department of Energy (DOE) [5]. Researchers at the University of Florida, studying the utilization of domestic fuels for hydrogen production, have found that ammonia-based solar-powered electrolysis produces the cheapest hydrogen (\$/GJ) compared to all other common hydrogen production technologies by the year 2024 [6]. Ammonia in alkaline media is oxidized at the anode (Eqn. 1) at a potential of -0.77 V versus standard hydrogen electrode (SHE). Alkaline reduction of water occurs on the cathode (Eqn. 2) and requires -0.83 V versus SHE. Overall (Eqn. 3), 0.06 V are required [3,7].

$$2NH_3(aq) + 6OH^- \rightarrow N_2(g) + 6H_2O + 6e^- \quad (1)$$

$$6H_2O + 6e^- \rightarrow 3H_2(g) + 6OH^- \quad (2)$$

$$2NH_3(aq) \rightarrow N_2(g) + 3H_2(g) \quad (3)$$

In addition to creating pure hydrogen and nitrogen with >99.99% Faradaic efficiency at room temperature and pressure [3], electrolyzing ammonia remediates nitrate contamination in ground and drinking water caused by human and animal excreta. These contaminations are believed to be an epidemic [8]. Current technologies used to desalinate nitrates from wastewater are expensive and have long retention times [9-12].

Ammonia-rich wastewater from breweries, tanneries, domestic wastewaters, landfills, fertilizer plants, brine wastewater, etc. are alkaline in nature [9, 12-15]. From an energetic and ecological point of view, ammonia electrolysis and optimization thereof could an important role in improving everyday life.

2.2.2 Electro-oxidation of ammonia: catalyst selection

Assuming negligible kinetic limitations during the electrolysis of ammonia at 25°C, 1.55 Wh per gram of hydrogen is required. This same gram of hydrogen theoretically generates 33 Wh from a proton exchange membrane fuel cell (PEMFC). Potentially, 31.45 Wh of net energy are available from an ammonia electrolytic cell (AEC) and PEMFC coupling. Thermodynamics of ammonia electrolysis is favorable; however, large anodic overpotentials have been observed on monometallic Pt electrodes [3, 7]. Given a PEMFC's 50-60% electrical efficiency [16, 17] and the increased energy consumption for ammonia electrolysis due to the electro-oxidation overpotential, the possible net energy from the coupling is threatened. There has been a significant amount of research regarding which catalyst(s) are best suited for ammonia oxidation. Noble transition metals such as Pt, Rh, Pd, and Ir have demonstrated to be active for ammonia oxidation whereas coinage metals like Cu, Ag, and Au are not [18, 19]. Electro-catalytic alloys and bimetallic depositions have proven to improve electro-kinetics of ammonia oxidation [3]. According to Moran *et al*. [19], a binary alloy of Pt-Ir has higher activity in alkaline media than other metals because Ir is the most selective metal for oxidizing

ammonia. Very limited research regarding this alloyed electro-catalyst in particular has been performed [3, 19-21], which is the aim of the present paper.

2.2.3 Objectives of the study

In the present paper, the most active electrocatalyst anode material for oxidizing ammonia in alkaline media at standard conditions was determined. Electroplating was the technique used for preparation of the electrodes. Within this context, the specific objectives of this paper are:

1. Determine the most active (minimal overpotential and maximum exchange current density) electrocatalyst for the electro-oxidation of ammonia in alkaline media using carbon fiber paper (CFP) electrodes depicted in Figure 2.1.
2. Optimize the plating bath of the most active electrocatalyst as well as the total catalytic loading based on geometrical surface area based on minimizing the climatic ammonia oxidation overpotential and exchange current density.
3. Quantify and qualify the electrode surface composition and morphology using scanning electron microscopy (SEM) and energy dispersive X-ray (EDX), respectively.

2.3 Experimental/materials and methods

2.3.1 Experimental setup and procedure

All chemicals and supplies were high purity (>99.9%) and supplied from Alfa Aesar or Fisher Scientific. A Solartron 1281 Multiplexer potentiostat was used for the

electrochemical studies throughout this paper. Statistical electrode optimization was accomplished using Stat-Ease Design Expert® 7.0. After studying the electrochemical performance of the electrodes, their surface morphology and atomic compositions were analyzed using a JEOL JSM-5300 SEM with a combined EDX from EDAX. Experimental errors were calculated using equipment uncertainties through propagation of error.

2.3.2 Electrode preparation

Figure 2.1 is a schematic representation of the electrodes used for this study. Electrodes were prepared similar to those presented in Figure 1 of Boggs and Botte [2]. Ti foil (0.127 mm thick, 99.9% pure from Alfa Aesar) acted as the current collector. It was cut with a pair of scissors so that a 2x2 cm^2 square was open. The remaining Ti on the sides (0.8 cm) of the square acted as arms, which were bent in half vertically. A sandwich-style packet 2.8 cm wide and 2 cm high containing two sheets of untreated Toray TGP-H-030 carbon fiber paper (CFP) with Ti gauze (18 mesh 99.9% pure Alfa Aesar) in between was placed in the square opening. Then, the half-vertically bent arms were closed and pressed holding the carbon fiber paper/Ti gauze packet in. Cellophane tape was used to mask the exposed Ti foil that is present in the plating bath. This was done to ensure that only the 2x2 cm^2 CFP was being deposited on. The electrodes were rinsed with acetone and HPLC-grade ultrapure water (Fisher Scientific). They were dried in an oven, and the electrode weights were recorded. This allowed for catalyst loading determination (electrode weight after plating minus electrode weight before plating).

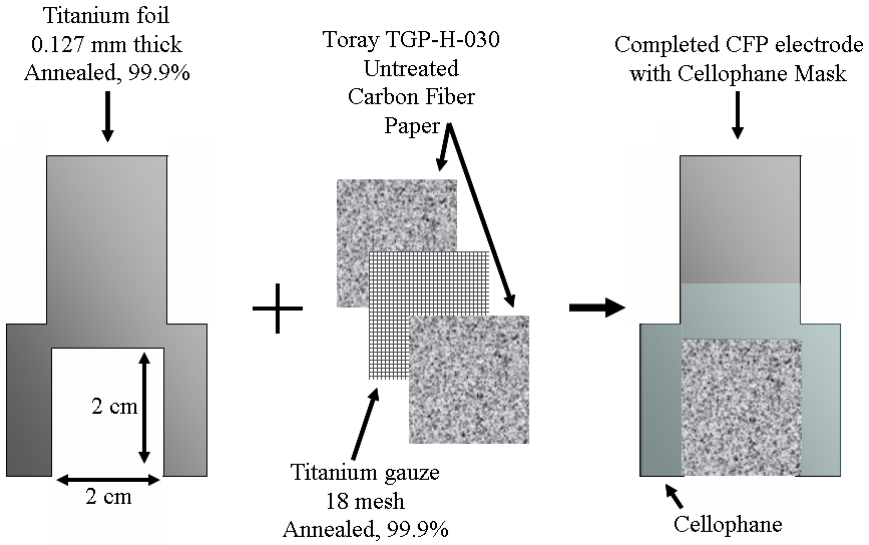

Figure 2.1: Schematic representation of electrodes used for this study. Titanium foil was cut to shape and a sandwich of CFP and Ti gauze were added. The Ti foil was then pressed enclosing the catalytic substrate sandwich. Titanium foil exposed to plating solution was masked using cellophane tape.

2.3.3 Anode catalyst – Objective 1

Table 2.1 shows the eight mono, bi, and ternary catalyst plating conditions. The concentration of each metal in the bath was 0.160 ± 0.001 g L^{-1}. All of the salts were 99.99% pure from Alfa Aesar. Deposition potentials were experimentally determined using cyclic voltammetry. The experiments were performed in the electrochemical cell shown in Figure 2.2. All electrodes in this study were plated potentiostatically with this same setup. A 2.5-cm stir bar at 60 rpm kept the bath solutions mixed during experimentation minimizing concentration gradients. Koslow Scientific supplied the Ag/AgCl reference electrode (+0.1999 V versus SHE) supported by a home-made Luggin capillary and filled with its respective electrolyte. The tip of the Luggin capillary was

placed 1 mm from the center of the working electrode. Platinum foil (0.01 cm thick, 99.999% pure from ESPI Metals) acted as the anode for plating except Ni. For plating Ni, Ni foil (0.127 mm thick, 99.9%) from Alfa Aesar was utilized. The Ni electrode was plated using the common Watts bath [22]. All of the plating solutions prepared for this paper were solvated with ultrapure high performance liquid chromatography (HPLC) water.

Table 2.1: Plating conditions for various metals

Metal	Anode (foil)	Electrolyte	Salts	Temperature (ºC)	Plating Potential (V versus Ag/AgCl)
Rh	Pt	1 M HCl/HPLC	$RhCl_3 \cdot 3H_2O$	78	-0.12
Ru	Pt	1 M HCl/HPLC	$RuCl_3 \cdot 3H_2O$	78	-0.12
Pt	Pt	1 M HCl/HPLC	$H_2PtCl_6 \cdot 6H_2O$	78	-0.12
Pt-Ir	Pt	1 M HCl/HPLC	$H_2PtCl_6 \cdot 6H_2O$ + $IrCl_3 \cdot 3H_2O$	78	-0.12
Ni	Ni	0.5 M $B(OH)_3$/HPLC	$NiSO_4 \cdot 7H_2O$ + $NiCl_2 \cdot 6H_2O$	45	-0.80
RhPt	Pt	1 M HCl/HPLC	$RhCl_3 \cdot 3H_2O$ + $H_2PtCl_6 \cdot 6H_2O$	78	-0.12
RuPt	Pt	1 M HCl/HPLC	$RuCl_3 \cdot 3H_2O$ + $H_2PtCl_6 \cdot 6H_2O$	78	-0.10
RhPtIr	Pt	1 M HCl/HPLC	$RhCl_3 \cdot 3H_2O$ + $H_2PtCl_6 \cdot 6H_2O$ + $IrCl_3 \cdot 3H_2O$	78	-0.11

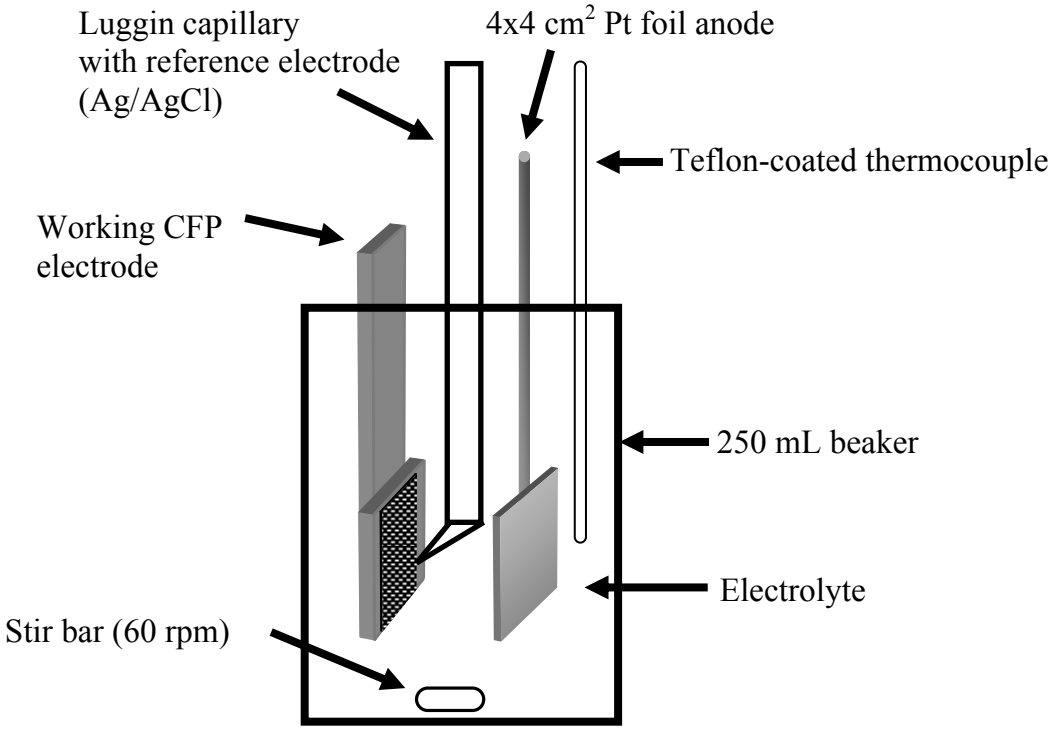

Figure 2.2: Electrochemical cell used for plating. Working and counter electrodes were held 3 cm apart. Table 2 shows electrolyte used depending on which metal is being deposited. Similar setup used for testing the electrodes in ammonia using a solution of 5 M KOH and 1 M NH_4OH.

2.3.4 Pt-Ir optimization matrix – Objective 2

A standard response surface methodology (RSM) with central composite design (CCD) was the statistical design of experiments used for this process optimization. CCD (shown in Figure 2.3) is a full factorial matrix at multiple levels that builds quadratic models for the response variables without the need of a complete three-level experiment and is the most common tool utilized for process optimization. The two responses of this design are the climatic ammonia oxidation overpotential (η) and exchange current density (i_o) both of which can be obtained from cyclic voltammograms. Minimizing the

overpotential will reduce the energy required for electrolysis and maximizing the exchange current density will increase kinetics [23, 24].

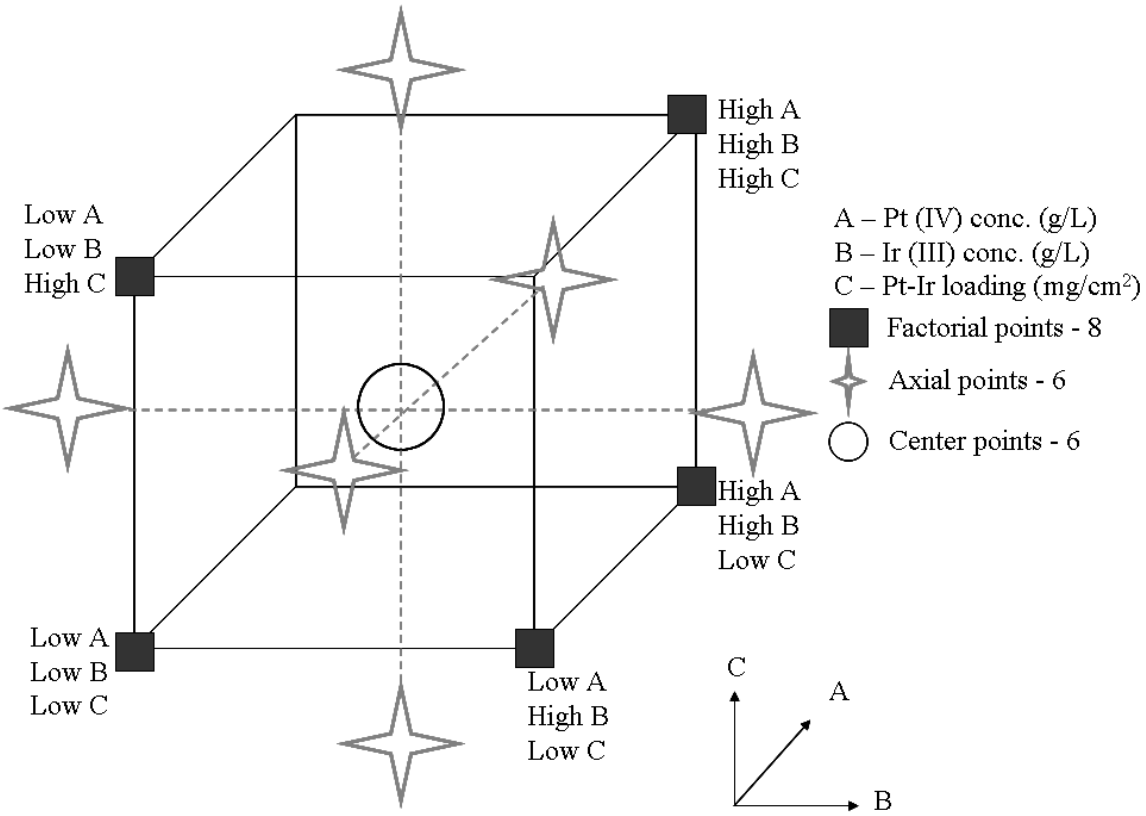

Figure 2.3: Schematic representation of statistical approach used for optimization. Central composite circumscribed (CCC) was the type of CCD used. Each corner of the square represents full factorial points. Stars represent axial points determined as a function of alpha. The central circle represents the six central points which are all at the same conditions making the system more robust [26].

Figure 2.4 shows how these two electrochemical characteristics are obtained from cyclic voltammetry. The overpotentials were obtained versus Hg/HgO accounting for 5 M KOH. The exchange current densities were obtained from the intercept of the Tafel plots (log current versus overpotential) taken from the forward scan of the oxidation of ammonia peak.

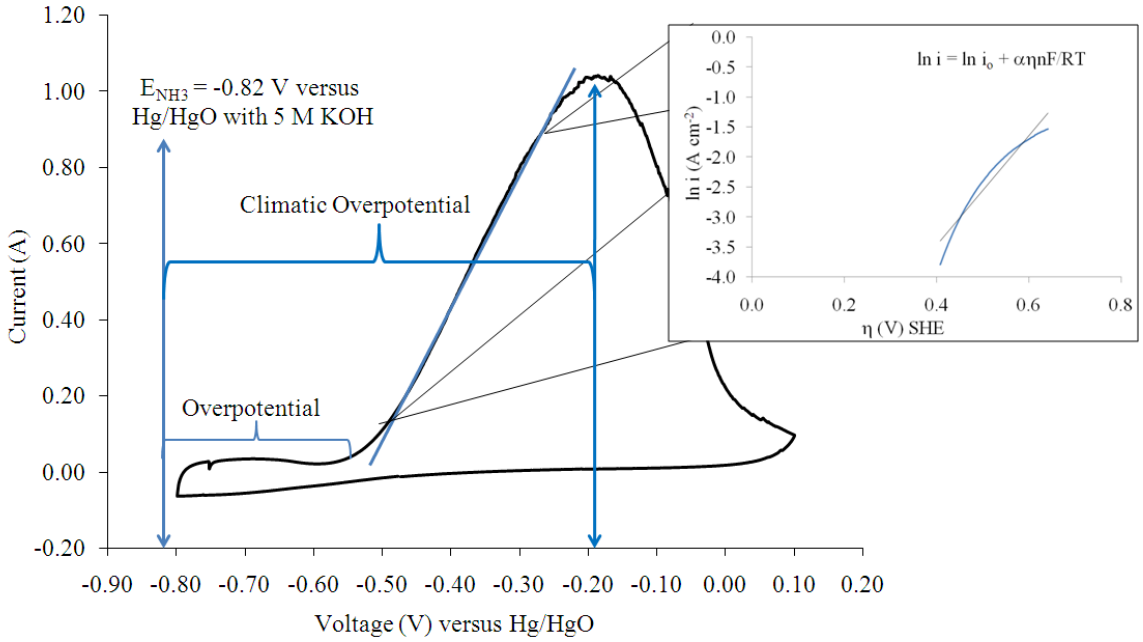

Figure 2.4: Methodology for analyzing ammonia oxidation overpotentials and exchange current densities using a cyclic voltammogram.

Pt (IV) concentration (g L^{-1}), Ir (III) concentration (g L^{-1}), and electro-catalyst loading (mg cm^{-2}) were the three factors optimized. A schematic representation of CCD is shown in Fig. 2.3. In addition to the typical "high" and "low" levels for test matrices, CCD uses a middle and two axial levels outside the "high" and "low" conditions. The experimental matrix is shown in Table 2.2. These levels were chosen based on prior knowledge of plating bath conditions and loadings [2, 7, 8]. The experiments were conducted over a two-day period in two blocks. Randomization was used to ensure any systematic effects that may have been present were transformed into experimental noise. Twelve runs (eight factorial points and 4 central points) occurred on Day 1. The remaining eight runs (six axial points plus 2 more central points) were held on Day 2. Axial points were chosen using a preset "alpha" of 1.41421 allowing the system to

remain rotatable. A rotatable system refers to the ability to rotate the design points about the center point and the moments of distribution of the design remain unchanged [25, 26].

Table 2.2: Pt-Ir CCD experimental matrix

Factor	Units	Low level (-1)	High level (+1)
A - Pt (IV) concentration	g L^{-1} (±0.001)	3.200	12.000
B - Ir (III) concentration	g L^{-1} (±0.001)	3.200	12.000
C - Pt-Ir Loading	mg cm^{-2} (±0.1)	5.5	20.0

Electrode	Block	Type	Bath Id	Factor A	B	C
1	Day 1	Factorial	1	3.200	3.200	5.5
2	Day 1	Factorial	2	12.000	3.200	5.5
3	Day 1	Factorial	3	3.200	12.000	5.5
4	Day 1	Factorial	4	12.000	12.000	5.5
5	Day 1	Center	5	7.600	7.600	12.8
6	Day 2	Axial	6	0.200	7.600	12.8
7	Day 2	Axial	7	15.000	7.600	12.8
8	Day 2	Axial	8	7.600	0.200	12.8
9	Day 2	Axial	9	7.600	15.000	12.8
10	Day 1	Factorial	1	3.200	3.200	20.0
11	Day 1	Factorial	2	12.000	3.200	20.0
12	Day 1	Factorial	3	3.200	12.000	20.0
13	Day 1	Factorial	4	12.000	12.000	20.0
14	Day 1	Center	5	7.600	7.600	12.8
15	Day 1	Center	5	7.600	7.600	12.8
16	Day 1	Center	5	7.600	7.600	12.8
17	Day 2	Axial	5	7.600	7.600	0.6
18	Day 2	Axial	5	7.600	7.600	24.9
19	Day 2	Center	5	7.600	7.600	12.8
20	Day 2	Center	5	7.600	7.600	12.8

2.4 Results and discussion

2.4.1 Active electrode geometric surface area

Figure 2.5 shows (a) a 3D image and (b) surface-depth analysis of the untreated Toray TGP-H-030 CFP chosen as catalytic support. In addition to its low cost and great physical properties, this substrate has a high ratio of surface area to volume and has exhibited minimal reactivity to a large range of operating conditions. These profiles were captured using an InfiniteFocus Light Microscope by Alicona. SEM imaging (c) shows that Pt-Ir deposits on both sides of the CFP support suggesting that total catalytic active area is 4 cm x 2 cm from the two exposed 2 cm x 2 cm sheets of CFP. See Figure 1 for reference. This area was used for current density and catalytic loading calculations.

(a)

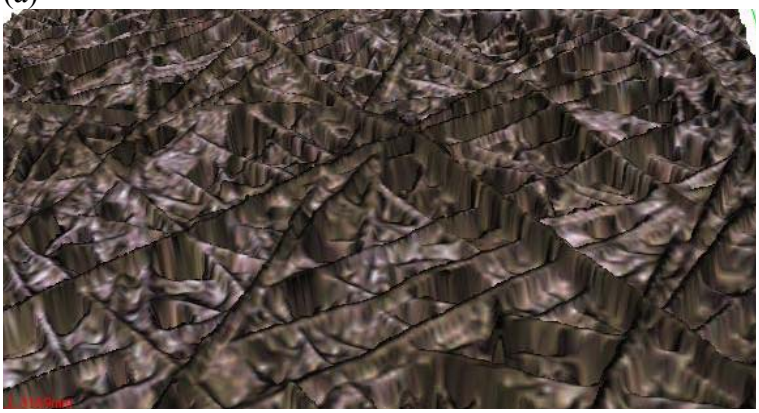

(b)

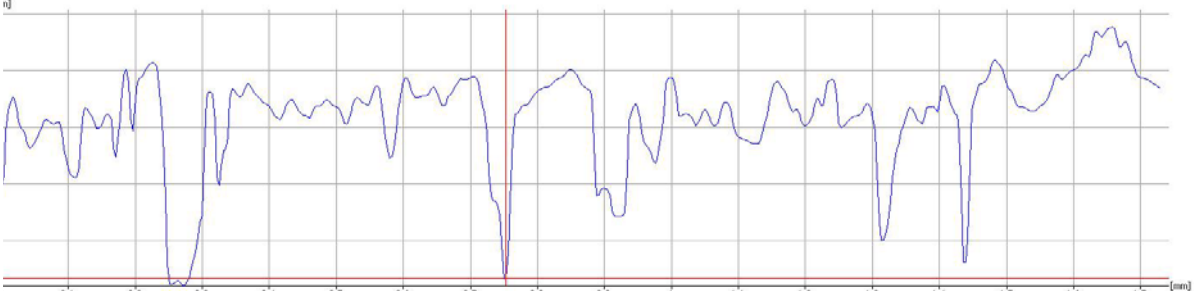

(c)

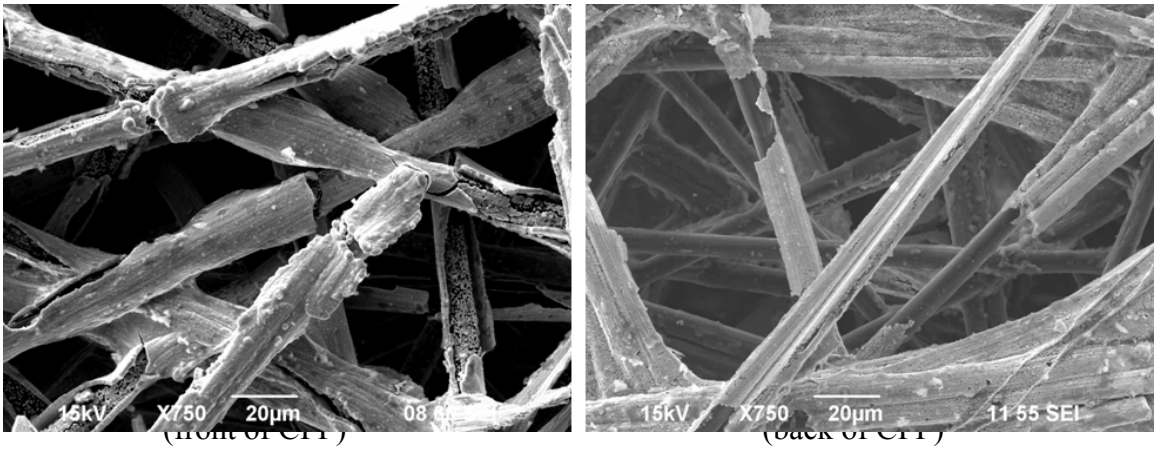

(front of CFP) (back of CFP)

Figure 2.5: Catalytic substrate analysis. (a) 3D surface image showing different surface heights echoed in the surface profile plot (b). (c) shows that metallic deposits occur completely throughout the CFP as well as the exposed surfaces.

2.4.2 Possible electro-catalysts for ammonia oxidation

Figure 2.6 shows cyclic voltammograms of possible electro-catalyst candidates for ammonia oxidation in alkaline media. Eight metals/combinations were studied. Carbon fiber paper electrodes shown in Fig. 2.1 were deposited with each respective metal/combination using the process parameters shown in Table 2.1. Electrodes were plated with 20 ± 0.1 mg. At first glance, Pt-Ir offers the largest exchange current density and second smallest ammonia oxidation overpotential based on Fig. 2.6.

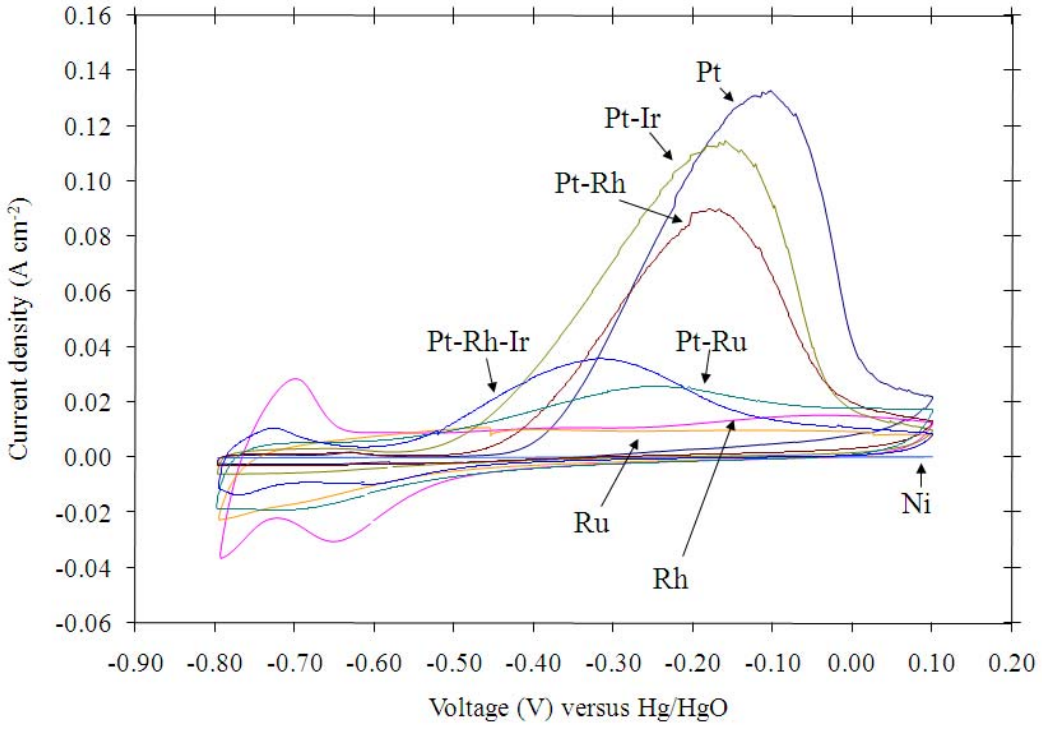

Figure 2.6: Anode metal comparison with cyclic voltammetry at 5 mV s^{-1} and 25°C. A 16 cm^2 Ni-foil counter electrode was used. Pt-Ir exhibited the best electrochemical behavior for oxidizing ammonia based on the criteria of minimizing ammonia oxidation overpotential and maximizing the Tafel slope.

Table 2.3 lists the metal/combinations along with their ammonia oxidation overpotentials versus Hg/HgO and exchange current densities. Ni-only, Rh-only, and Ru-only did not show signs of oxidizing ammonia which is echoed by Ge and Johnson [18] and Moran *et al.* [19]. In terms of minimizing the ammonia oxidation overpotential, catalyst selection is ranked as follows Pt-Ir-Rh > Pt-Ru > Pt-Rh > Pt-Ir > Pt. With regards to maximizing the exchange current density, the ranking is Pt-Ir > Pt-Rh > Pt > Pt-Ir-Rh > Pt-Ru. Due to the large exchange current density and average oxidation overpotential, Pt-Ir was chosen as the most active and suitable electrocatalyst to further optimize.

Table 2.3: Anodic metal comparison for the electro-oxidation of ammonia in alkaline media

Catalyst	η (mV) vs SHE (±0.1)	i_o (mA cm^{-2}) (±0.1)
Rh	738.4	0.4
Ru	749.4	0.3
Pt	498.6	6.2
Ni	698.1	0.3
Pt-Ir	394.9	9.3
Pt-Rh	455.1	7.4
Pt-Ru	440.6	1.0
Pt-Ir-Rh	366.0	2.5

2.4.3 Pt-Ir plating bath optimization

The experimental matrix in Table 2.2 yielded nine different plating bath compositions in terms of Pt (IV) and Ir (III) concentrations. Figure 2.7 shows plating bath characterization by cyclic voltammetry for each of the nine different baths in order

to obtain a constant plating potential for the study. Based on the results of Fig. 2.7, electrodes for Pt-Ir optimization were plated at a constant plating potential of -0.12 V versus Ag/AgCl. New baths were prepared for each of the twenty electrodes in Table 2.2 to ensure Pt (IV) and Ir (III) concentration changes did not affect deposition behavior.

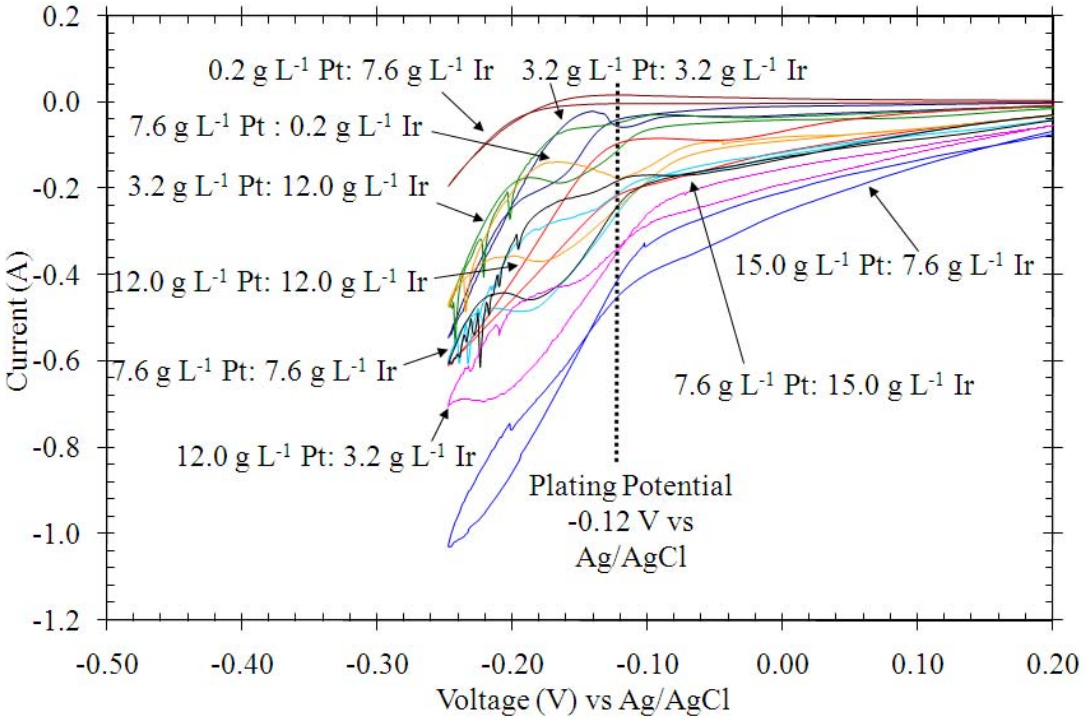

Figure 2.7: Plating potential characterization for Pt-Ir optimization experimental matrix. Cyclic voltammetry was used with a voltage scan rate of 5 mV/s. The solutions were stirred at 60 rpm and temperature controlled at 78°C. A 16 cm^2 Pt foil was used for the anode.

Table 2.4 shows the overpotential and exchange current densities for the design matrix. Also included are the atomic compositions of Pt and Ir. Plating bath efficiencies were calculated based on the atomic composition of Pt.

Table 2.4: Experimental matrix results including atomic surface compositions and plating efficiencies

Electrode	Factors			Climatic η (mV) vs SHE (±0.1)	i_o (mA cm^{-2}) (±0.1)	Atomic Composition (%) (±0.2)		Plating efficiency η (%) (±0.4)
	A	B	C			Pt	Ir	
1	3.200	3.200	5.5	727.4	0.8	67.4	33.5	50.1
2	12.000	3.200	5.5	387.4	6.0	74.4	26.4	60.5
3	3.200	12.000	5.5	457.7	1.2	53.7	47.9	34.6
4	12.000	12.000	5.5	587.0	1.6	55.3	45.8	33.3
5	7.600	7.600	12.8	831.3	7.6	78.0	22.4	85.3
6	0.200	7.600	12.8	625.8	1.0	40.1	60.6	26.1
7	15.000	7.600	12.8	872.8	9.9	64.7	36.7	44.3
8	7.600	0.200	12.8	819.1	2.4	72.9	28.1	60.4
9	7.600	15.000	12.8	685.0	2.6	69.6	31.2	51.0
10	3.200	3.200	20.8	723.7	5.1	75.9	25.6	64.4
11	12.000	3.200	20.8	809.6	9.4	70.1	30.4	52.1
12	3.200	12.000	20.0	677.7	2.5	57.4	43.8	46.3
13	12.000	12.000	20.0	754.9	4.4	56.4	44.7	42.9
14	7.600	7.600	12.8	697.9	2.0	51.8	49.6	43.4
15	7.600	7.600	12.8	741.3	3.5	61.1	39.1	51.8
16	7.60	7.600	12.8	730.4	1.5	77.4	23.0	61.7
17	7.60	7.600	0.6	649.7	0.1	65.4	35.0	48.0
18	7.60	7.600	24.9	712.4	3.9	60.7	40.8	43.6
19	7.60	7.600	12.8	679.5	1.3	68.8	32.4	62.8
20	7.60	7.600	12.8	680.4	1.7	61.1	39.2	45.7

The atomic composition of Pt and the plating efficiency are a function of one another. This is verified in Fig. 2.8 which shows that the plating efficiency is higher with proportional increase in the atomic composition of Pt. Also, there is a proportional trend between the ammonia oxidation overpotential and the loading. Similarly, an increase in surface composition of Pt leads to an increase in exchange current densities while an increase in Ir surface composition decreases the ammonia oxidation overpotential. Based on these tradeoffs, optimization of the bath is necessary.

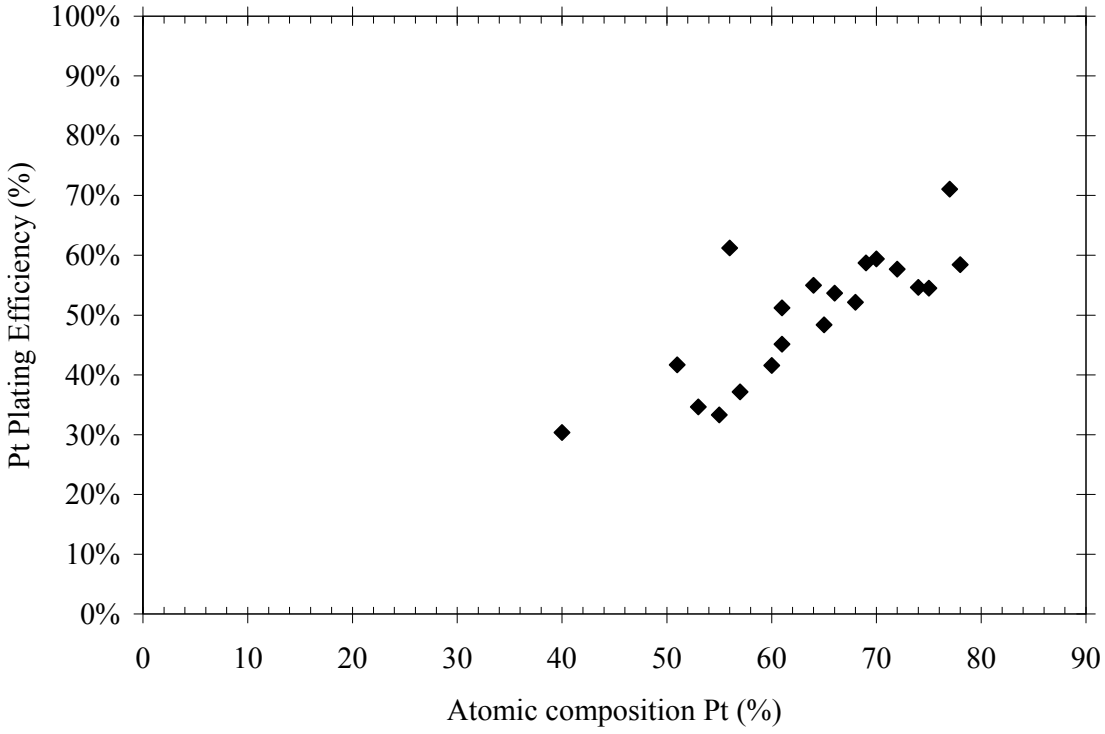

Figure 2.8: As the Pt atomic composition of the electrode increases, so does the plating efficiency. This is based on Pt only suggesting that the deposition of Ir decreases the plating efficiency.

Energy dispersive x-ray spectroscopy was used for each electrode as well. EDX confirmed that Pt-Ir bimetallic alloy had been plated on each electrode. Figure 2.9 (a) shows spectrum plots of Electrode 2 before and after depositing Pt-Ir. Figure 2.9 (b) shows EDX color mapping of the electrode elements present as well as elemental distribution.

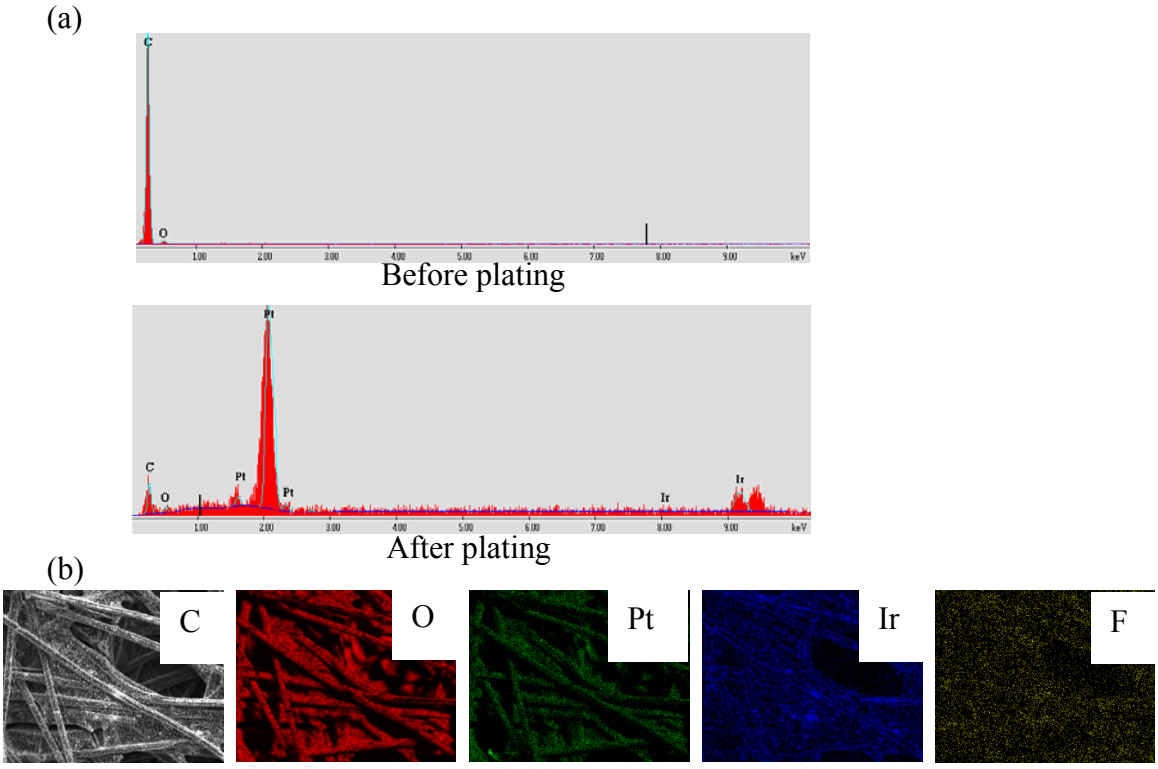

Figure 2.9: Energy dispersive x-ray spectroscopy. Working distance 10 mm, dead time 20%: (a) spectrum plot of Pt-Ir electrodes before and after plating; (b) color mapping showing elemental distribution of the electrode's surface.

Using the response data in Table 2.4 in Stat-Ease Design Expert® 7.0, statistical models for each response were generated. Equation 5 is the linear response model for the oxidation of ammonia overpotential. Equation 6 is the quadratic model response for the exchange current density of Pt-Ir in alkaline ammonia electrolysis. A is the Pt(IV) concentration (g L^{-1}), B is the Ir(III) concentration (g L^{-1}), and C is the catalytic loading (mg cm^{-2}) of Pt-Ir. Table 2.5 shows ANOVA analysis for both responses.

Table 2.5: ANOVA results for the system responses. Both models suggested are significant according to a 95% confidence interval.

Response	Source	p-value (Prob > F)	Comment
Climatic η (mV) vs SHE	Model	0.0002	*Significant*
	A - Pt conc.	0.0002	
	B - Ir conc.	0.0024	
	C – Loading	0.3032	
	Lack of Fit	0.9399	*Not significant*
i_o (mA cm^{-2})	Model	0.0124	*Significant*
	A-Pt conc.	0.0646	
	B – Ir conc.	0.0204	
	C – Loading	0.0442	
	AB	0.0417	
	AC	0.0143	
	BC	0.2857	
	Lack of Fit	0.0706	*Not significant*

$$\eta_{NH3} = 0.65 + 0.056A - 0.042B + 0.013C \qquad \textbf{(5)}$$

$$i_o = 3.42 - 0.31A - 0.89B + 0.53C - 0.73AB - 2.45AC + 0.97BC \qquad \textbf{(6)}$$

Figure 2.10 (a) shows the evenly distributed normalized residual plot for ammonia oxidation overpotential, and (b) shows residual plot for the exchange current densities. Using the optimization software described by Myers [24], each response yielded the optimum plating process parameters. An overall process desirability of 0.690 was achieved for minimizing ammonia oxidation overpotential and maximizing exchange current density of ammonia electrolysis. Stat-Ease® combines individual response desirabilities into one process desirability. A value of 1.000 indicates an ideal case. Optimized process parameters are summarized in Table 2.6. Figure 2.11 is a 3D plot of the optimized process parameters as a function of desirability.

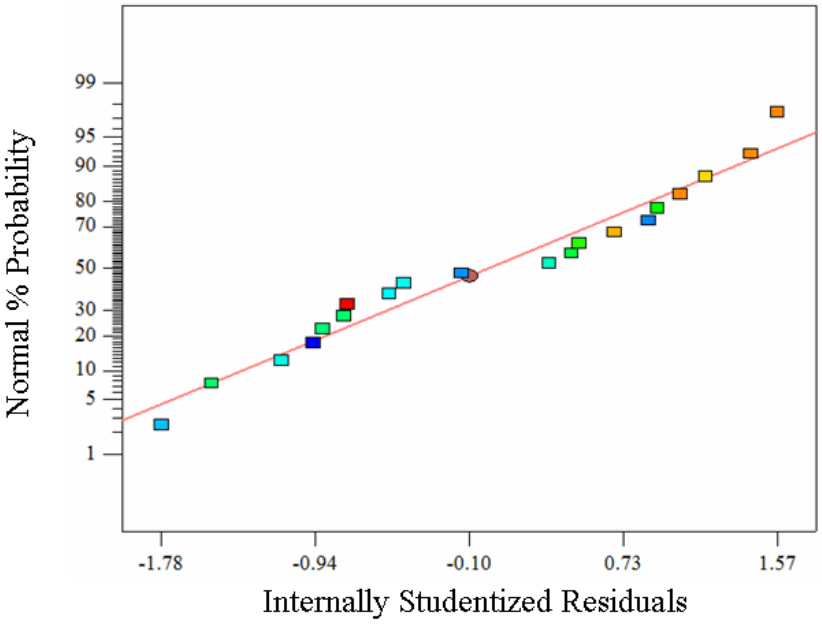

(a)

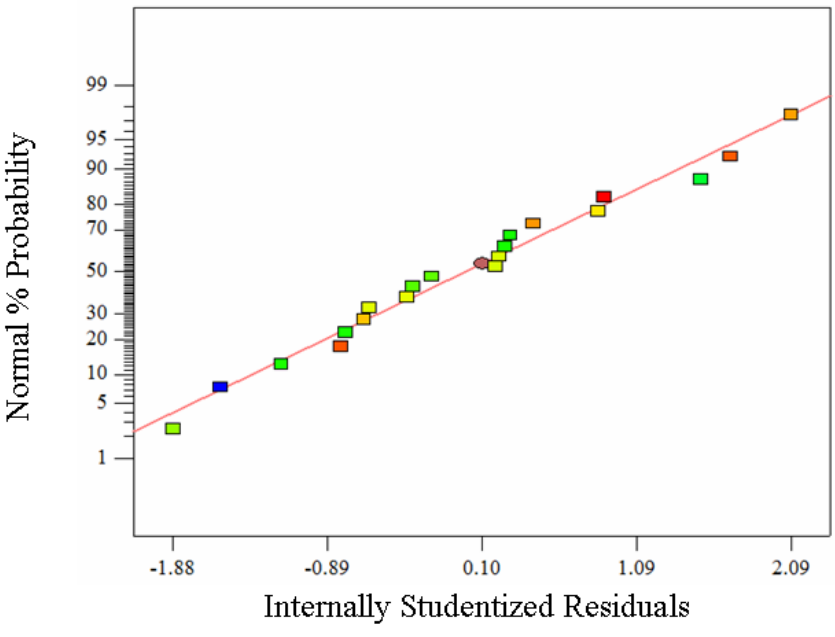

(b)

Figure 2.10: Normal probability plots for experimental matrix factors: (a) climatic ammonia oxidation overpotential; (b) ammonia oxidation Tafel slope. The data points are approximately linear indicating desired normality in the error term.

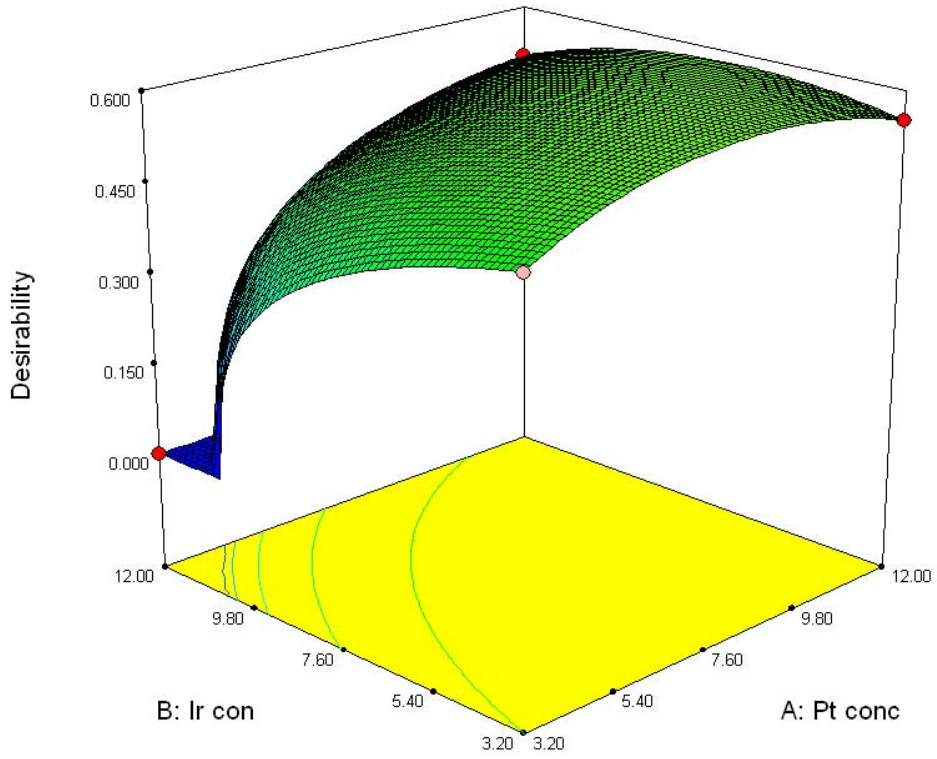

Figure 2.11: 3D response surface plot at a catalytic loading of 5.5 ± 0.1 mg cm^{-2}. Optimization of the plating process parameters indicate that plating bath of 8.844 ±0.001 g L^{-1} Pt (IV) and 3.20 ± 0.001 g L^{-1} Ir (III) should be used to obtain a minimal ammonia oxidation overpotential and maximum Tafel slope.

.

Table 2.6: Numerically optimized process conditions for plating CFP anodes based on desirability.

Pt (g L^{-1}) (±0.001)	Ir (g L^{-1}) (±0.001)	Loading (mg cm^{-2}) (±0.1)	η (mV) V SHE (±0.1)	i_o (mA cm^{-2}) (±0.1)	Desirability
8.844	4.112	5.5	682.4	5.1	0.690

2.5 Conclusions

Pt-Ir as an anode catalyst is the most suitable material for oxidizing ammonia in alkaline media. The concentrations of the Pt-Ir plating bath play a major role in the electrochemical behavior of oxidizing ammonia as well as the overall catalytic loading. These factors have been optimized for producing electrodes that will electrolyze ammonia with the lowest ammonia electrooxidation overpotential and largest exchange current density. Optimized process parameters are summarized in Table 6. As a result, lower energy is consumed during electrolysis and faster kinetics is accomplished. It is recommended that a narrower Pt-Ir loading window between 0.1 and 5 mg cm^{-2} be optimized using the optimized plating bath conditions found Table 6.

2.6 References

[1] G. Thomas, G. Parks. *Potential roles of ammonia in a hydrogen economy: A study of issues related to the use of ammonia for on-board vehicular hydrogen storage.* U.S. Department of Energy (2006).

[2] B.K. Boggs, G.G. Botte**.** J. Power Sources **192** (2009)**.**

[3] F. Vitse, M. Cooper, G.G. Botte. J. Power Sources **142** (2005).

[4] G. G. Botte, F. Vitse, M. Cooper, *Electrocatalysts for the Oxidation of Ammonia and Their Application to Hydrogen Production, Fuel Cells, Sensors, and Purification Processes*, US Patent 7,485,211, (2004).

[5] S. Satyapal, J. Petrovic, C. Read, G. Thomas, G. Ordaz. Catal. Today 120 (2007).

[6] S.T. Mirabal, H.A. Ingley, N. Goel and Y. Goswami. Int. J. Power Energy Syst **24** (2004).

[7] M. Cooper, G.G. Botte**.** J. Mater. Sci. **41** (2006).

[8] E. Bonnin, E. Biddinger, G.G. Botte. J. Power Sources **182** (2008).

[9] C. Alfafara, T. Kwawmori, N. Nomura, M. Matsumura. J. Chem. Technol. Biotechnol. **79** (2004).

[10] D.C. Bouchard, M.K. Williams, R.Y. Surampalli**.** J. Am. Water Works Assn. **84** (1992).

[11] A.F. Bouwman, D.S. Lee, W.A.H. Asman, F.J. Dentener. Global Biogeochem. Cycles **11** (1997).

[12] K. Vijayaraghavan, D. Ahmad, R. Lesa**.** Ind. Eng. Chem. Res. **45** (2006).

[13] L. Shao, P. He, J. Xue, G. Li. Water Sci. Technol. **53** (2006).

[14] L. Szpyrkowicz, S. N. Kaul, R. N. Neti, S. Satyanarayan. Water Res. **39** (2005).

[15] A.G. Vlyssides, P.K. Karlis, N. Rori, A.A. Zorpas. J. Hazard. Mater. **95** (2002).

[16] J.J. Hwang, D.Y. Wang, N.C. Shih. J. Power Sources **141** (2005).

[17] M.W. Melaina. Int. J. Hydrogen Energy **28** (2003).

[18] J.S. Ge, D.C. Johnson**.** J. Electrochem. Soc. **142** (1995).

[19] E. Moran, C. Cattaneo, H. Mishima, B.A. López de**.** J. Solid State Electrochem. **12** (2008).

[20] K. Endo, Y. Katayama, T. Miura**.** Electrochim. Acta **50** (2005).

[21] K. Endo, K. Nakamura, Y. Katayama, T. Miura**.** Electrochim. Acta **49** (2004).

[22] J.P. Hoare**.** J. Electrochem. Soc. **133** (1986).

[23] P.T. Kissinger, W.R. Heineman, Laboratory Techniques in Electroanalytical Chemistry, 2nd ed., Marcel Dekker Inc., New York, NY, 1984.

[24] C.M.A. Brett, A.M.O. Brett, Electrochemistry: Principles, Methods, and Applications. Oxford, 1993.

[25] M.J. Anderson, P.J. Whitcomb, RSM Simplified: Optimizing Processes Using Response Surface Methodology for Design of Experiments. Productivity Press, New York, NY, 2005.

[26] R.H. Myers, Response Surface Methodology. Allyn and Bacon Inc., Boston , MA, 1971.

CHAPTER 3.

ON-BOARD HYDROGEN STORAGE AND PRODUCTION: AN APPLICATION OF AMMONIA ELECTROLYSIS

It should be noted that the contents of this chapter are published in a peer-reviewed journal: B.K. Boggs and G.G. Botte, *J. Power Sources*, **192,** 2, p. 573-581 (2009).

3.1 Abstract

On-board hydrogen storage and production via ammonia electrolysis was evaluated to determine whether the process was feasible using galvanostatic studies between an ammonia electrolytic cell (AEC) and a breathable proton exchange membrane fuel cell (PEMFC). Hydrogen-dense liquid ammonia stored at ambient temperature and pressure is an excellent source for hydrogen storage. This hydrogen is released from ammonia through electrolysis, which theoretically consumes 95% less energy than water electrolysis; 1.55 Wh per gram of H_2 is required for ammonia electrolysis and 33 Wh per gram of H_2 for water electrolysis. An ammonia electrolytic cell (AEC), comprised of carbon fiber paper (CFP) electrodes supported by Ti foil and deposited with Pt-Ir, was designed and constructed for electrolyzing an alkaline ammonia solution. Hydrogen from the cathode compartment of the AEC was fed to a polymer exchange membrane fuel cell (PEMFC). In terms of electric energy, input to the AEC was less than the output from

the PEMFC yielding net electrical energies as high as 9.7 ± 1.1 Wh g^{-1} H_2 while maintaining H_2 production equivalent to consumption.

3.2 Introduction

3.2.1 On-board hydrogen production

Interest in hydrogen fuel-cell vehicles (HFCVs) has been increasing in popularity over the past decade. This is primarily a result of the shrinking oil reserves which are expected to last only 42 years as of 1998 [1]. HFCVs have also found a niche in the environmental and political fields because they offer a solution for eliminating the harmful air pollutants generated by internal combustion engines (ICEs) such as nitrogen oxides (NO_x), volatile organic compounds (VOCs), carbon dioxide (CO_2), and sulfur dioxide (SO_2) [2-4]. In addition to being environmentally friendly, HFCVs are quiet and convert 50-60% of the energy available in hydrogen to power the automobile rather than the 20-30% efficiency of today's hydrocarbon-dependent vehicles [5, 6].

A hydrogen future is not only driven by the transportation sector but as a movement for reducing oil imports in general and eliminating the dependence on petroleum for daily energy production. HFCVs as personal transportation vehicles are believed to be the best alternative. They have high efficiencies, emit no harmful pollutants, and can operate in cold temperatures unlike battery-powered vehicles (BPVs) [7, 8]. However, storing enough hydrogen that allows a fuel-cell vehicle to travel the same range as today's ICEs between refueling is proving difficult and delaying the commercialization and market approval of HFCVs. Compared to gasoline, hydrogen has

2.7 times more energy content based on weight However, due to its tremendously low density, hydrogen has 25% less energy content than gasoline when based on volume [9]. Because of this, there is no storage technology currently available that allows a vehicle to travel the average 482-km range that today's internal combustion engines obtain [10].

As a result, research on producing hydrogen on board has accelerated. Generating hydrogen on board in a manner that does not produce air pollutants and requires the small amount of energy available from renewable sources is the definite long-term solution [3]. This is where *in situ* ammonia electrolysis enters the picture.

3.2.2 Ammonia and electrolysis

Liquid ammonia is a non-carbon containing hydrogen-dense (17.6 wt.%) fuel that can be stored at ambient temperature and pressure [11]. Theoretically, ammonia electrolysis requires 95% less energy than water electrolysis (1.55 Wh g^{-1} H_2 versus 33 Wh g^{-1} H_2). In fact, Vitse *et al*. state that hydrogen produced from the electrolysis of ammonia costs \$0.89 per kg of H_2 opposed to \$7.10 per kg of H_2 from water electrolysis. These numbers were based on an ammonia cost of \$275 per ton and a solar energy cost of \$0.214 per kWh [12]. This low cost is single-handedly a result of the low energy consumption of ammonia electrolysis. The U.S. Department of Energy's (DOE's) targeted cost of hydrogen for 2015, per kg of hydrogen or gallon of gasoline equivalent (gge), is \$2-3 [10]. Ammonia electrolysis has other uses besides generating hydrogen for mobile applications such as nitrate desalination at domestic wastewater treatment plants, electrochemical sensors, and for the production of nitrogen [12-14].

$$2NH_3(aq) + 6OH^- \rightarrow N_2(g) + 6H_2O + 6e^- \quad (1)$$

$$6H_2O + 6e^- \rightarrow 3H_2(g) + 6OH^- \quad (2)$$

$$2NH_3(aq) \rightarrow N_2(g) + 3H_2(g) \quad (3)$$

At the anode (Eqn. 1), ammonia is electro-oxidized and has a potential of -0.77 V versus standard hydrogen electrode (SHE). Alkaline reduction of water occurs on the cathode and requires -0.83 V versus SHE. Overall, Eqn. 3, 0.06 V are required. This makes ammonia electrolysis attractive for producing hydrogen when comparing the required 1.23 V for water electrolysis according to the thermodynamics at standard conditions [12].

There is criticism when discussing the possibilities of using ammonia as a source of hydrogen storage that is echoed in the DOE position paper that discusses the use of ammonia for onboard storage. This DOE paper only discusses the feasibility of ammonia thermal cracking rather than other novel ammonia-hydrogen technologies such as electrolysis. Cracking ammonia requires temperatures greater than 500°C, ammonia purification equipment to prevent ammonia poisoning of fuel cells, and a complex system [11]. Alkaline fuel cells (AFCs) could use the ammonia-doped hydrogen reducing the threat of poisoning, but these fuel cells require operating temperatures ranging from 65°C to 220°C [15]; as a result, the overall energy requirements increase. On the other hand, ammonia electrolysis and the hydrogen-air polymer exchange membrane fuel cell (PEMFC) process requires ambient temperature and pressure. Also, little or no ammonia purification equipment for the fuel cell is required because the cathode side of the AEC (where H_2 is generated) only needs to be in contact with KOH.

Another criticism is the availability of ammonia. According to the DOE, ammonia has been produced for more than 100 years economically using the Haber-Bosch process. Also, there are more than 4,800 km of ammonia distribution pipelines that spreads over much of central U.S. allowing distribution costs of ammonia to be similar to liquid petroleum gasoline (LPG) distribution costs [11]. Even more convincing, nearly 54 million metric tons of gas-phase ammonia is emitted into the atmosphere world wide annually. Major sources include domestic animal excreta (40.2%), synthetic fertilizers (16.7%), oceans (15.2%), burning of biomass (10.9%), crops (6.7%), human excreta (4.8%), soils under vegetation (4.4%), and industrial processes (0.6%) [16]. It's safe to assume, especially for the excreta sources, that the liquid-phase ammonia, which is generating much of the gas, is higher in concentration. According to McCubbin *et al*., gas-phase ammonia emissions contribute to the formation of ammonium nitrate and sulfate. They found that these particulate emissions can result in a variety of health problems including: asthma attacks, chronic bronchitis, and even premature mortality and suggested that a 10% reduction in ammonia emissions would save $4 billion dollars in health costs each year [17]. Moreover, nitrate contamination of groundwater is largely due to liquid-phase ammonia emissions from both human and animal excreta. Too much exposure to nitrates can lead to methemoglobinemia, which prevents the transport of oxygen by the blood. As a result, the U.S. Environmental Protection Agency (EPA) has limited the nitrate contamination level in drinking water to 10 mg L^{-1}. This is believed to be a pandemic and remediation costs are high [18].

Basakcilardan-Kabakci *et al*. [19] has demonstrated that 97% of ammonia present in urine can be captured through stripping and absorption. Even more promising, urea present in urine is easily hydrolyzed to ammonium increasing the amount of ammonia present in urine. Moreover, naturally occurring enzymes called urease decomposes urea to ammonia by the following reaction [20]:

$$NH_2(CO)NH_2 + 2H_2O \rightarrow NH_3 + NH_4^+ + HCO_3^- \quad (4)$$

Utilizing this free ammonia as hydrogen storage, results in an estimated $0.33 per kg of H_2 theoretically; this does not include the stripping and absorption equipment used to capture the ammonia. Essentially, ammonia can be called a biofuel. It's difficult to compare to other biofuels such as ethanol because the sewer-to-ammonia-to-wheel efficiency is much higher than the ammonia-to-fertilizer-to-corn-to-ethanol-to-wheel cycle that ethanol faces. Plus, ethanol-combusting vehicles emit the same air pollutants as today's automobiles and depend heavily on climate conditions [21].

Thermodynamically for one gram of H_2, ammonia electrolysis consumes 1.55 W h. For this same gram of H_2, a PEMFC, which is the reverse reaction of water electrolysis, generates 33 Wh. After sending 1.55 Wh back to the AEC from the PEMFC, making the system self sustaining, there is potential for a net energy of 31.45 Wh that can be used to recharge the batteries used for system start-up, to power a motor, or for any other applications. However, PEMFCs have efficiencies that range from 50-60% [5, 6]. Additionally, ammonia is converted to hydrogen with 100% Faradaic efficiency, but kinetic problems creating large ammonia oxidation overpotentials exist [12].

The focus of this paper is on-board hydrogen production with *in situ* ammonia electrolysis. The goal is to determine whether or not using liquid-ammonia as hydrogen storage and electrolyzing it to obtain the hydrogen is a viable hydrogen storage technology compared to the 2010 technical targets set forth by the DOE [10]. Within this context, there are three objectives:

1. Develop an anode and cathode for the AEC. The Electrochemical Engineering Research Laboratory (EERL) at Ohio University, has demonstrated that combinations of Pt and Ir minimized the overpotential of the electro-oxidation of ammonia resulting in a decrease in power consumption during electrolysis compared to other metals such as Ru, Rh, Ni, and combinations thereof [12, 22, 23].
2. Design and construct a static alkaline ammonia electrolytic cell. An AEC, that separates hydrogen from the cathode from the nitrogen generated at the anode, was constructed.
3. Determine the feasibility of using ammonia for on-board vehicular hydrogen storage. Synergistic analysis was performed on the AEC and PEMFC. This was carried out using polarization techniques allowing for energy consumption and generation data to be obtained.

3.3 Experimental/materials and methods

3.3.1 Electrode preparation

Figure 3.1 shows the schematic diagram for the preparation of the electrodes. The anode and cathode base were 3.7 cm × 4.7 cm 18 mesh titanium gauze (0.28 mm diameter wire and 100% purity from Alfa Aesar). Ti gauze served as the current

collector for the untreated Toray TGP-H-030 (0.11 μm thick and 80% porosity) carbon fiber paper (CFP) catalytic substrate. The gauze and CFP were supported with titanium foil (0.127 mm thick, annealed, and 99% purity from Alfa Aesar). Titanium was chosen due to its chemical resistance to the acidic environment present during electroplating and the alkaline electrolyte used for testing.

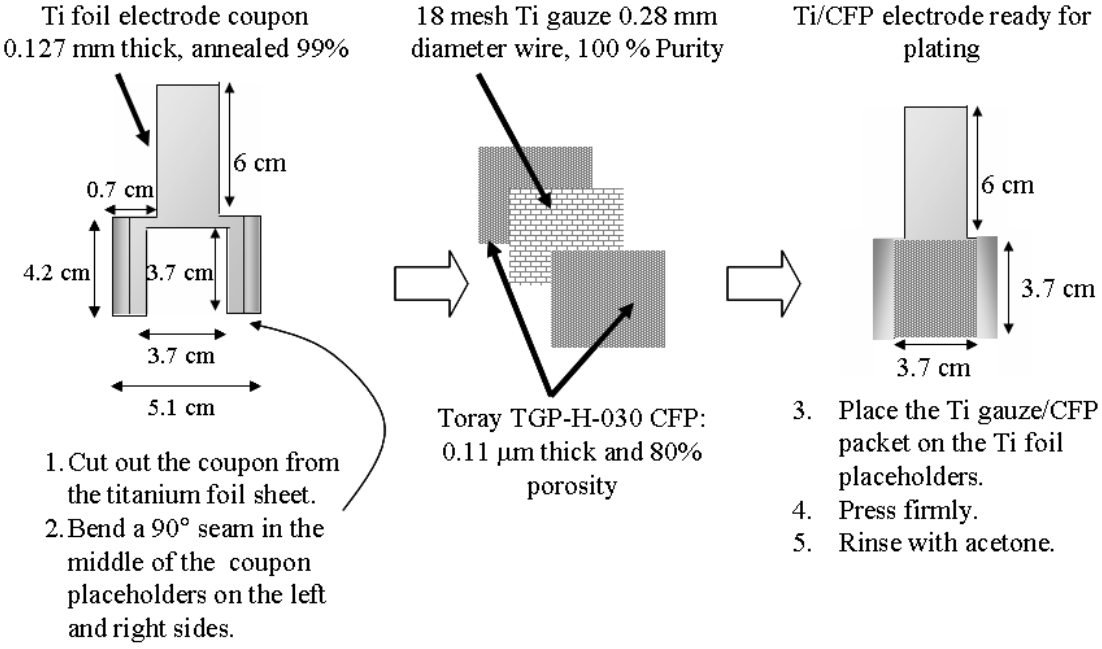

Figure 3.1: Schematic representation of the procedure used for the preparation of the carbon fiber paper electrodes. Titanium foil was used as the Ti gauze and CFP support. Ti gauze was used as the current collector to increase the electronic conductivity of the carbon fiber paper.

Ti gauze was placed between two 3.7 cm × 4.7 cm sheets of CFP. Then, the electrodes were pressed and rinsed with acetone to remove any greasy compounds that may have formed during construction. Overall, the active catalytic surface area for each

electrode was 27.4 cm^2. Finally, the electrodes were dried and weighed before and after electroplating to determine the catalytic loadings.

Electroplating was carried out in a 250 mL beaker that contained 1 M HCl (99.5% pure 6 N from Fisher Scientific) solvated with high performance liquid chromatography (HPLC) water from Alfa Aesar. This solution was temperature controlled at 78°C with constant stirring at 60 rpm using a 2.5 cm magnetic stir bar. The platinum and iridium salts were dihydrogen hexachloroplatinate (IV) ($H_2PtCl_6 \cdot 6H_2O$ – 38% Pt) and iridium chloride ($IrCl_3$ – 55% Ir) from Alfa Aesar, respectively. The purity of both salts was 99.9% (metal basis). Salt concentrations were 2.4 g L^{-1} H_2PtCl_6 and 4.8 g L^{-1} $IrCl_3$. The anode was 4 cm × 4 cm Pt foil (0.102 mm thick 99.95% from ESPI Metals).

The potentiostatic voltage used for plating Pt-Ir was -0.077 V versus Ag/AgCl. It took 1.6 hours to deposit 339.4 ± 0.1 mg of Pt-Ir alloy on the anode yielding an average Faradaic plating efficiency of 13.4% based on Pt only since Ir is extremely difficult to deposit alone. Similarly, it took 1.7 hours to deposit 355.2 ± 0.1 mg on the cathode with a 12.6% plating efficiency.

Figure 3.2 shows scanning electron microscopy (SEM) images of the CFP before plating and anode and cathode CFP after plating. The electrocatalyst loading per mg of geometric surface area was chosen based on the point before the Pt-Ir alloy particles begin to agglomerate and diminish surface area. Figure 3.2a is the CFP before plating, Figure 3.2b is the anode after plating and after characterizing in ammonia solution (this explains why some of the Pt-Ir deposit has come off in the micro-image), and Figure 3.2c is the cathode after plating and testing. On average, the particles ranged between 200-

300 nm in diameter according to SEM. When electroplating the bimetallic Pt-Ir alloy, the following reductions occur and based on these reduction potentials, iridium can be deposited along with platinum [24, 25]. E^0 is referenced to standard hydrogen electrode (SHE):

$$PtCl_6^{2-}(aq) + 4e^- \rightarrow Pt(s) + 6Cl^-(aq) \quad E^0 = 0.744V \tag{5}$$

$$Ir^{+3}(aq) + 3e^- \rightarrow Ir(s) \quad E^0 = 1.156V \tag{6}$$

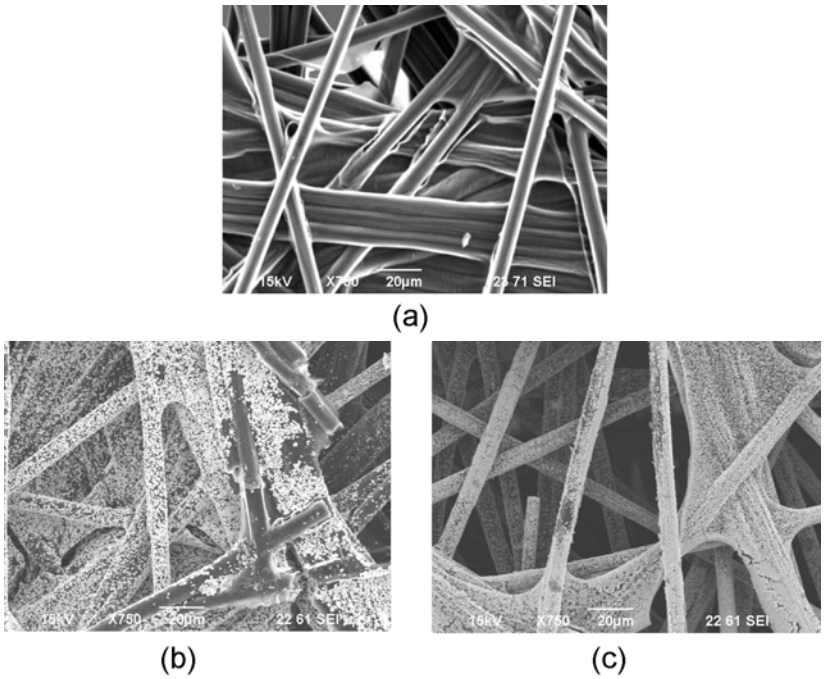

Figure 3.2: Scanning electron photomicrographs. Magnification 750X, voltage: 15 kV: (a) Toray TGP-H-030 CFP before plating; (b) anode after plating; (c) cathode after plating

The optimum loading of Pt-Ir on this CFP for the electrolysis of ammonia is currently being investigated at the EERL. For the purposes of this paper, 12.4 mg cm^{-2} is an adequate loading ensuring low energy consumption of the AEC.

3.3.2 Ammonia electrolytic cell design and construction

A sandwich configuration was used for the AEC. Fig. 3.3 shows the details of the cell design. Main components of the cell are: cast acrylic endplates, ethylene propylene diene monomer (EPDM) rubber gaskets, membrane, and Ti/CFP anode and cathode. These materials were chosen based on their chemical resistance to the alkaline electrolyte present during electrolysis.

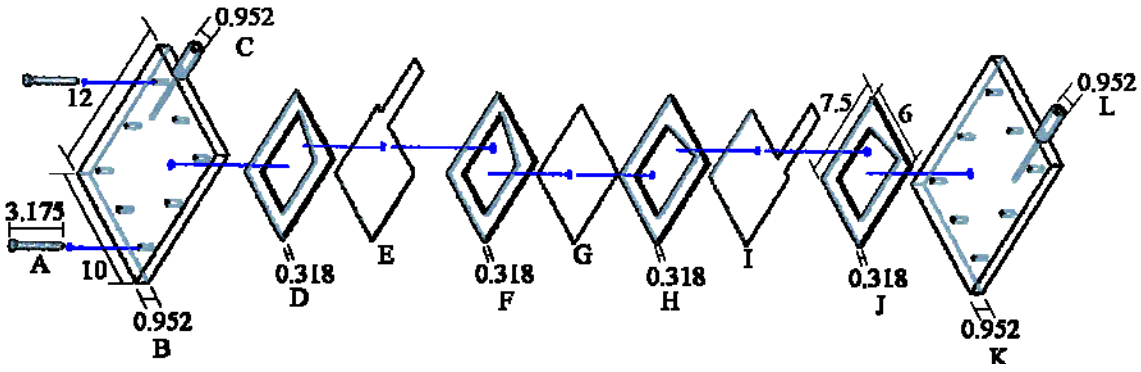

Figure 3.3: Schematic representation of the ammonia electrolytic cell (AEC). A sandwich configuration was used, and the parts include: 6-32 stainless steel screws and nuts (A), acrylic plates (B and K), hollow acrylic rods (C and L), ethylene propylene diene monomer (EPDM) gaskets (D, F, H, and J), working and counter electrodes (E and I), and gas separator (G). The channels machined in the acrylic endplates, for both gas collection and holding the cell together using the stainless steel screws, are 0.32 cm in diameter. All dimensions shown are given in cm.

Cast acrylic plates (11 cm × 13 cm and 0.95 cm thick) and 0.32 cm thick EPDM (4.7 cm × 4.7 cm) were purchased from McMaster-Carr. A hydrophilic Teflon membrane from W.L. Gore Associates was used as the gas separator. The electrolytic cell was made of a sandwich configuration with the two acrylic endplates holding the electrode/gasket/membrane assembly between them. The cell was tightened ensuring no leaks using stainless steel screw and nuts. Channels (3.175 mm in diameter) were machined at the top of the endplates for the gases to be collected. Also, 8 holes (3.175 mm in diameter) were drilled around the perimeter of the endplates for the stainless steel screws. Since this is a static configuration, there were intermediate bubbles exiting the endplates rather than a continuous flow that a PEMFC desires.

3.3.3 AEC and PEMFC integration study

In order to determine the feasibility of *in situ* ammonia electrolysis as an on-board hydrogen generating technology, a synergistic analysis of the AEC and PEMFC was required. Figure 3.4 shows a schematic representation of the integration experiment.

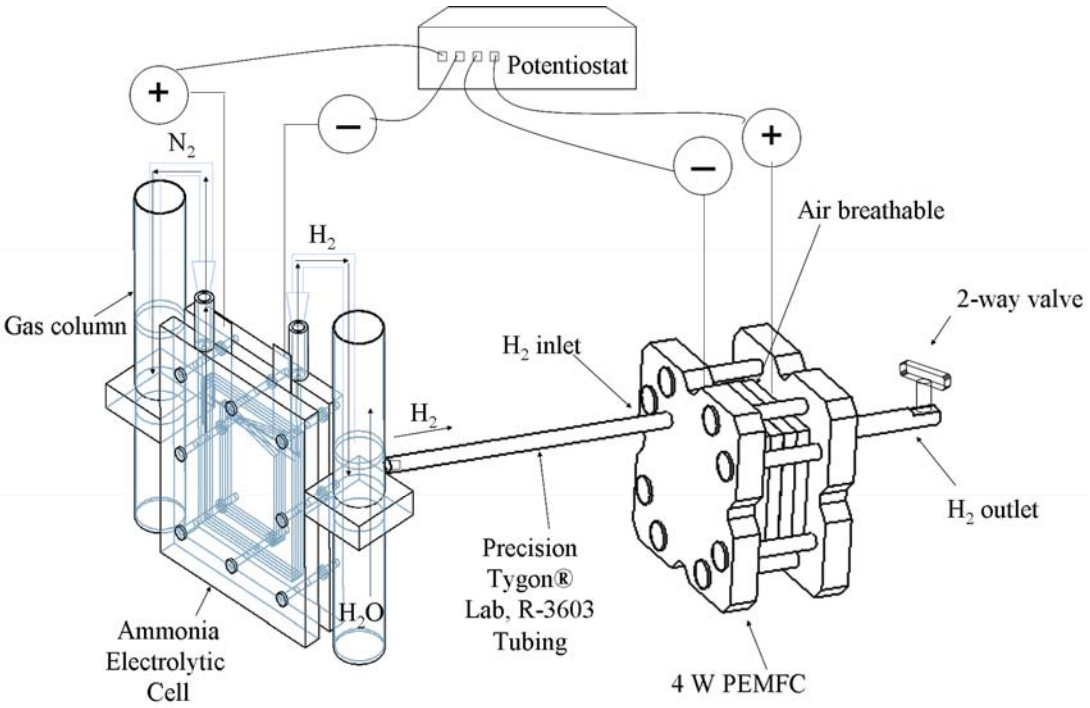

Figure 3.4: Schematic diagram of the AEC-PEMFC integration set-up. All integration experiments were performed with this configuration.

Gas collection columns, which can be seen on the AEC in Fig. 3.4, were added to both compartments which displace water to the top as the gases exit the AEC; this also pressurizes both compartments equally which allowed the gas to leave the AEC easier. Only one milliliter of hydrogen was required for storage creating a small hydrostatic pressure that helps keep a continuous flow of hydrogen entering the fuel cell. The study was performed using a multi-channel Arbin cycler BT2000. An electrolyte consisting of 5 M KOH was added to the cathode side of the AEC while a solution of 1 M NH_4OH and 5 M KOH was added to the anode. An air-breathable 4 W 5-cell PEMFC from Parker was used.

Before testing, the PEMFC needed to be purged of any air [27]. In order to accomplish this, a simple two-way valve (McMaster-Carr) placed on the hydrogen outlet of the PEMFC was closed. Then, 500 mA was applied to the AEC until 12 mL of hydrogen was produced (10 mL in the gas collection cylinder + 2 mL in the tubing connecting the hydrogen-side of the AEC to the PEMFC). The hydrogen-outlet valve was then reopened purging any air that may have been present in the H_2 gas collection column and PEMFC. Then, the valve was closed again making the proceeding tests dead ended.

For characterizing the PEMFC at various loads to obtain hydrogen consumption rates, 500 mA was applied to the AEC until 12 mL of hydrogen was produced and stored. Then the AEC was shut off. Amperic loads ranging from 100 mA to 400 mA in 50 mA increments were applied to the PEMFC individually to determine the hydrogen consumption rate (mL min^{-1}). Faraday's Law was then used to determine the AEC currents required to generate hydrogen at the same rate of consumption [28]:

$$m = \frac{MIt}{nF} \tag{7}$$

Where M is the molecular weight of hydrogen, I is the applied current, t is the time over which the experiment is conducted, n is the number of electrons transferred, and F is the Faradaic constant (96,485 C). Fortunately, ammonia electrolysis has a 100% Faradaic efficiency [12]. So, the currents predicted from Faraday's Law were tested while simultaneously applying the respective loads to the fuel cell to determine if the system could produce hydrogen at the same rate it was consumed. Experiments were performed at 25°C and 1 atm. Cell potentials for both the AEC and PEMFC were

recorded automatically by the potentiostat attaining electric energy consumption and generation data. Based on these data, the feasibility of net energy was determined.

3.4 Results and discussion

3.4.1 Integration analyses

Figure 3.5 shows the hydrogen consumption rates of the 4 W PEMFC at various loads. The error bars shown were calculated using propagation of error based on the experimental uncertainties of the instrumentation and glassware used.

At a 400 mA load, transport losses dominated. It's important to note that the operating pressure of the hydrogen for the setup in Fig. 3.4 was atmospheric and less than the manufacturer's suggested 0.14 atm. Table 3.1 shows the AEC currents required to maintain hydrogen production equivalent to consumption by the PEMFC.

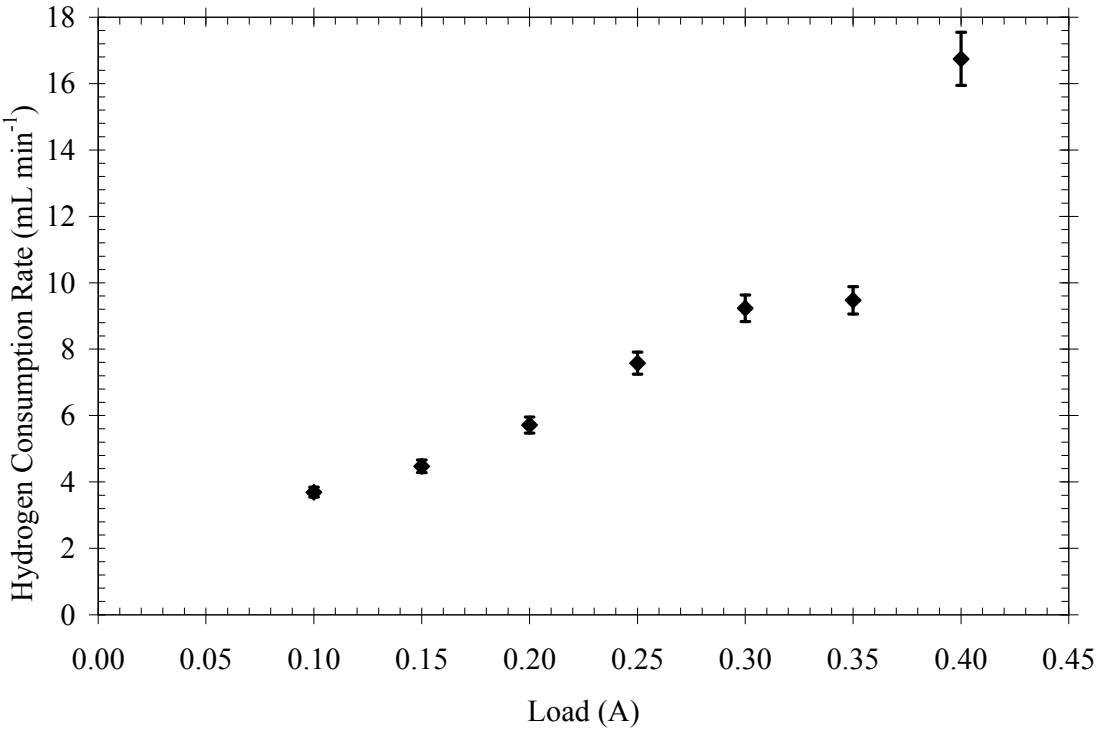

Figure 3.5: Hydrogen consumption rates for the PEMFC at various loads using the experimental setup shown in Fig. 3.4.

Figure 3.6 shows the energy efficiencies of both the AEC and PEMFC based on thermodynamics. AEC electrical efficiency is low based on the fact that the theoretical energy is only 1.55 Wh per gram of hydrogen versus the 33 Wh per gram of hydrogen theoretical energy for PEMFCs.

$$\eta_{AEC} = \frac{Actual\ Energy\ Consumption}{1.55\frac{Wh}{g}} \tag{8}$$

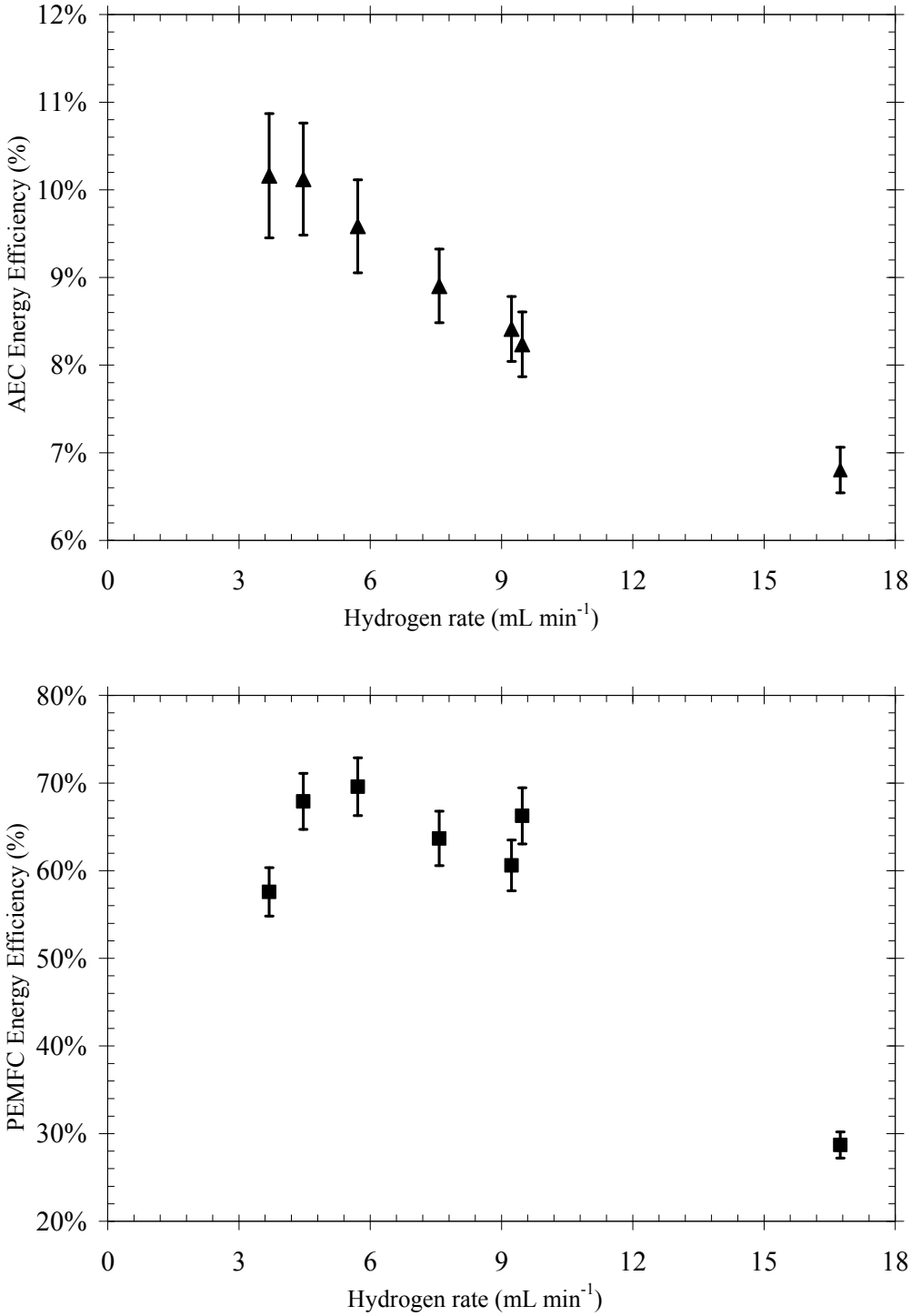

Figure 3.6: Energy efficiencies based on thermodynamics at 25°C: (top) AEC; (bottom) PEMFC

Table 3.1: AEC currents required to maintain hydrogen production equivalent to consumption

PEMFC Load (A) ± 0.001	PEMFC Voltage (V) ± 0.0001	Required AEC Current (A) ± 0.001	AEC Voltage (V) ± 0.0001
0.100	4.1632	0.525	0.5232
0.150	3.9642	0.650	0.5564
0.200	3.8931	0.825	0.5877
0.250	3.7804	1.085	0.6274
0.300	3.6511	1.325	0.6659
0.350	3.5120	1.360	0.6824
0.400	2.3532	2.400	0.8450

Figure 3.7 shows that the AEC is only consuming 60% of the energy generated from the PEMFC at standard quiescent conditions. It's safe to assume using the heat generated from an electric motor in an automobile in addition to the heat produced from a PEMFC would yield even higher AEC-PEMFC net energies. In order to demonstrate a self-sustaining capability, the hydrogen production rate must equal the consumption rate. Using the PEMFC as air breathable has limitation on the load.

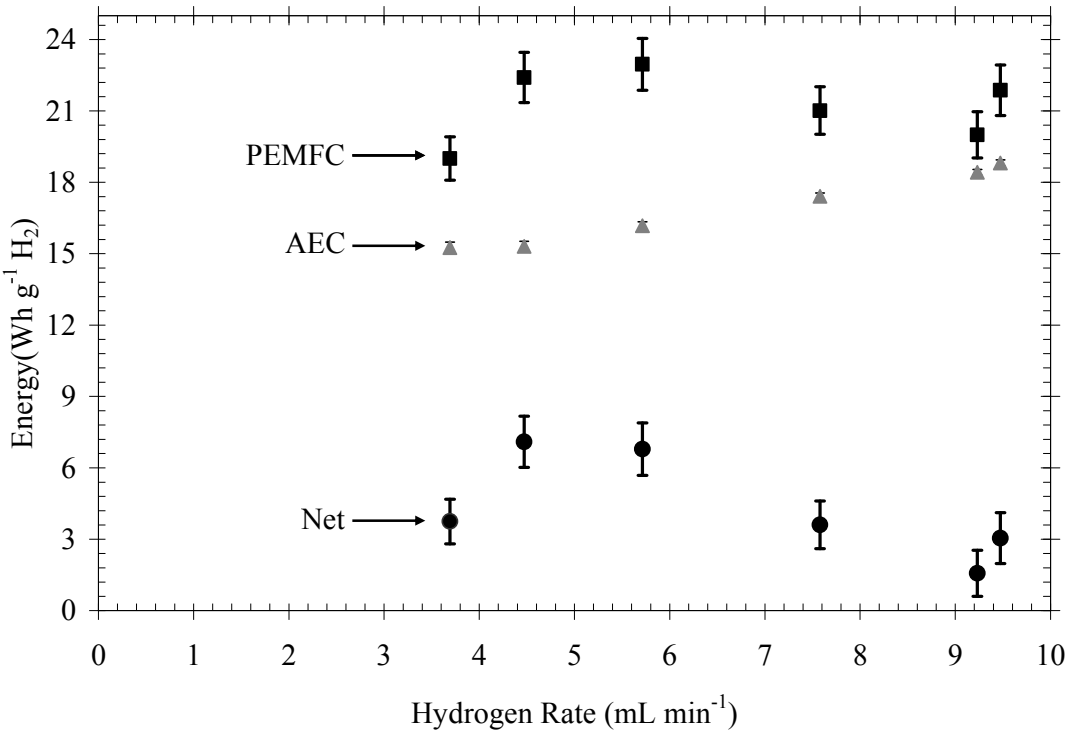

Figure 3.7: Net electrical energies from AEC-PEMFC integration analysis preformed at standard conditions.

According to the manufacturer, 300 mA can be withdrawn before transport losses heavily influence the cell's performance. Due to these transport losses in the fuel cell, a negative net energy ensued while withdrawing 400 mA and was eliminated from Fig. 3.7. For all the other loads, where transport losses within the PEMFC were not observed, there were net electric energies as high as 9.7 ± 1.1 Wh g^{-1} H_2.

3.4.2 Feasibility analysis of ammonia electrolysis as an on-board hydrogen storage system

Figure 3.8 shows a process layout for an on-board hydrogen storage system using ammonia electrolysis. Components of the system which constitute as storage are the

ammonia storage tank, AEC, start-up hydrogen drum to maintain a continuous flow of hydrogen to the fuel cell, compressor, PEMFC, process control, and tubing.

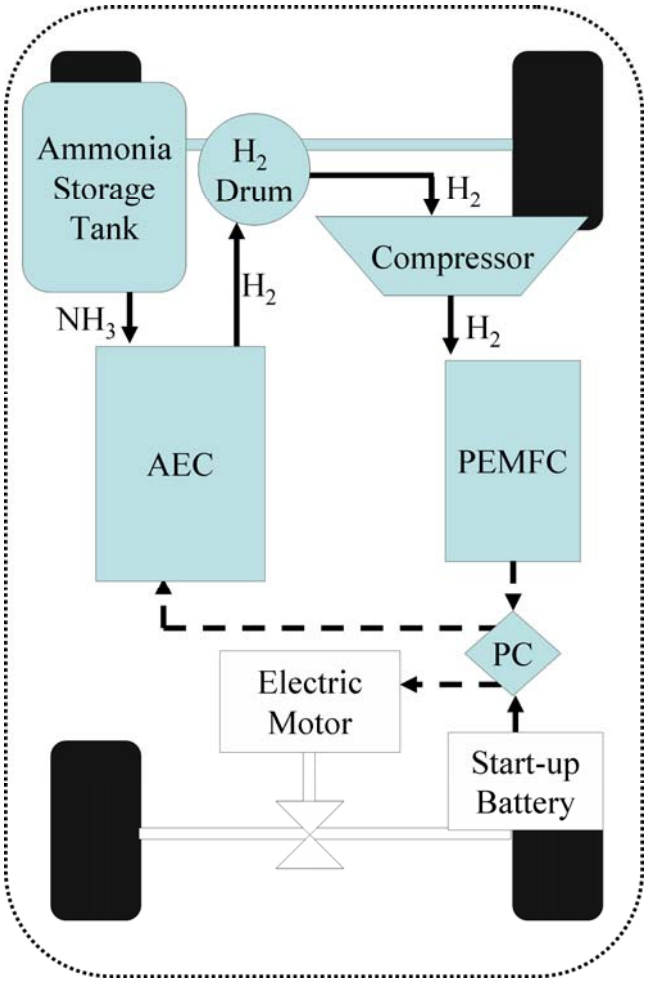

Figure 3.8: Schematic representation of an on-board hydrogen storage system using ammonia electrolysis: The components that make up the storage part for this system are : (1) ammonia storage vessel with ammonia fuel; (2) Teflon tubing; (3) ammonia electrolytic cell; (4) start-up hydrogen drum; (5) compressor; (6) PEMFC; and (7) process control.

Other alternative designs that can be optimized to further meet DOE storage parameter targets are possible. These seven major components in Fig. 3.8 were used to estimate the storage parameters (system gravimetric capacity, system volumetric capacity, and storage system cost) set by the U.S. DOE. This was done to compare ammonia electrolysis storage parameters to the 2010 technical targets set forth by the DOE's FreedomCAR and Fuel Partnership [10]. The results are shown in Table 3.2.

The following is an individual description of the seven major components required for an ammonia electrolytic process that explains, in detail, the basis for calculating storage parameters. First, liquid ammonia needs to be stored similarly to that of liquid petroleum gasoline [11]. A lightweight and chemical resistant polymer composite tank from Advanced Lightweight Engineering was used for the design. Second, the tubing to be used is 12.7-cm diameter Teflon tubing from McMaster-Carr. It is approximated that 3 m would be required. Third is the ammonia electrolytic cell. A pump is not required between the storage tank and AEC because the vapor pressure of stored ammonia is high enough to push itself through the electrolyzer. A controller is proposed to manage the amount of ammonia entering the AEC depending on the demand from the PEMFC. It is essentially hydrogen on demand. In addition, since ammonia electrolysis has proven to be 100% efficient, a recycle line of un-reacted ammonia is not required. Fourth, in order for the automobile to be self-sustaining until ammonia is depleted, the fuel cell needs to be powerful enough to run the automobile as well as the electrolyzer. Based on the results shown in Fig. 3.7, at the highest net energy, the AEC is consuming 60% of the PEMFC's energy. This means that a 69 kW PEMFC is required

to meet AEC energy requirements as well as the 483-km range requirement. Fig. 3.9 shows the energy balance for a HFCV using ammonia electrolysis. Appendix A shows that 41 kW of this PEMFC is used as part of storage based on the fact that the AEC is consuming 60% of the PEMFC's energy.

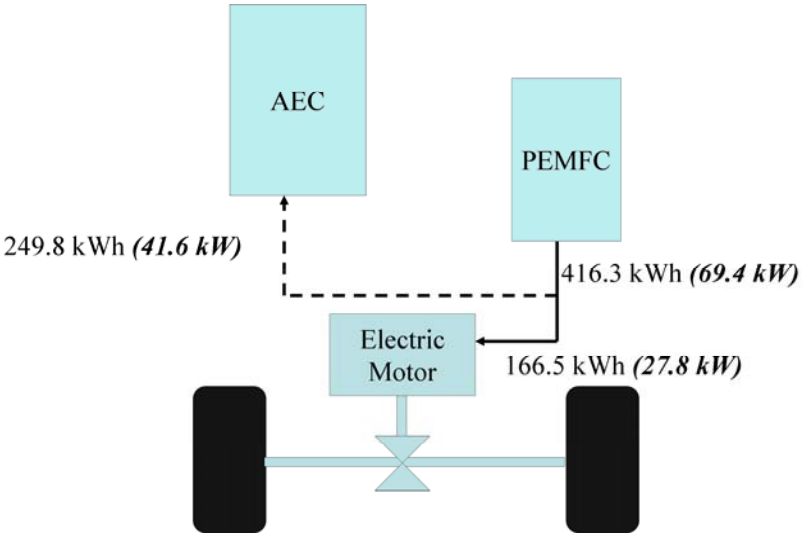

Figure 3.9: Balance of plant in terms of energy for a HFCV utilizing in situ ammonia electrolysis as hydrogen storage at 25°C.

Since the AEC configuration is similar to that of a PEMFC, it was assumed that the AEC weight and volume is approximate to twice the weight and volume of the PEMFC. Once the PEMFC generates enough energy to power the AEC and motor, a start-up battery, used to establish steady state, can be turned off. As a result, this enables a vehicle to be self sustaining and obtain the 483-km range between refueling. Fifth, a start-up hydrogen collection drum will be necessary to ensure the compressor has a continuous flow of hydrogen. A simple high-density polyethylene storage drum from McMaster-Carr was used for storage parameter estimation. Sixth, the compressor weight,

volume, and cost were based on the compressor targets in the 2005 *Fuel Cell Technology Road Map* set forth by the FreedomCAR and Fuel Partnership [29]. Finally, process control involves taking power from the PEMFC and sending it to the ammonia electrolytic cell and motor. It was determined through AEC and PEMFC synergistic analysis that ammonia electrolysis is most stable at galvanostatic conditions rather than potentiostatatic, so transforming the voltage from the fuel cell to current is necessary. An average engine computer from Autoparts Giant was used to estimate the cost. Details of the calculations and cost analysis can be found in Appendix A.

The weight, volume and cost of 41 kW PEMFC, which is accounted for in the ammonia electrolysis storage system, was determined based on the parameters from the *Fuel Cell Technology Road Map* [29]. When calculating the cost of hydrogen ($/kg), an ammonia cost of $0.36 per kg was used. This cost would be significantly lower if human and animal waste from domestic wastewater treatment plants and agricultural runoff were used.

In Table 3.2, despite operating at worst-case conditions (quiescent and room temperature), it appears that ammonia electrolysis as a storage system meets most of the technical targets set forth by the DOE. System gravimetric and volumetric capacities based on energy are lower than the DOE targets because 60% of the PEMFC is accounted for as part of the storage target calculations. On the other hand, the gravimetric and volumetric capacities based on the amount of hydrogen are exceeded. Having a self-sustaining vehicle however makes some of these numbers seem inconsequential. Figure 3.10 shows that improving current density of the electrodes significantly decreases the

storage system costs. Presently, 130 mA cm^{-2} is achieved; however, if 2,200 mA cm^{-2} were achieved, then the DOE's storage cost for 2010 would be met. Reducing the number of electrodes by increasing the current density will also improve gravimetric and volumetric parameters for using ammonia.

Table 3.2: Storage parameters for a HFCV using ammonia electrolysis

Storage Parameter	Units	Ammonia Electrolysis	2010 DOE Target
System Gravimetric Capacity	kWh/kg system	1.8	2.0
	kg H_2/kg system	0.09	0.06
System Volumetric Capacity	kWh/L system	1.2	1.5
	kg H_2/L system	0.059	0.045
Storage System Cost	$/kWh net	88	4
	$/kg H_2	1,742	133
Fuel Cost	$/gge* at pump	2.02	2.00-3.00

*gallon of gasoline equivalence (gge)

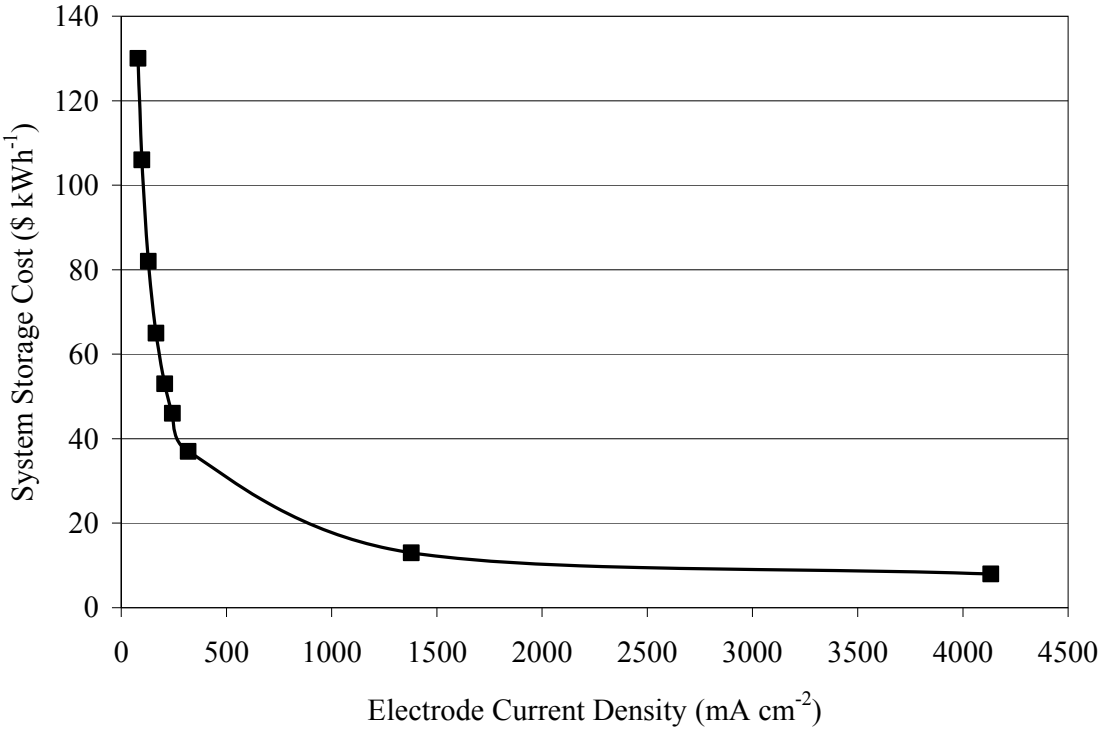

Figure 3.10: Sensitivity analysis on the effect of electrode current density and the system storage cost. A steep decent in system storage costs with a small improvement in electrode current density is observed.

There is a linear relationship between the cost of ammonia and cost of hydrogen generated on board as shown in Fig. 3.11. The cost of ammonia is dependent on the cost of natural gas; however, the cost of ammonia can go as high as $0.53 per kg before the cost of hydrogen exceeds the DOE target for 2010.

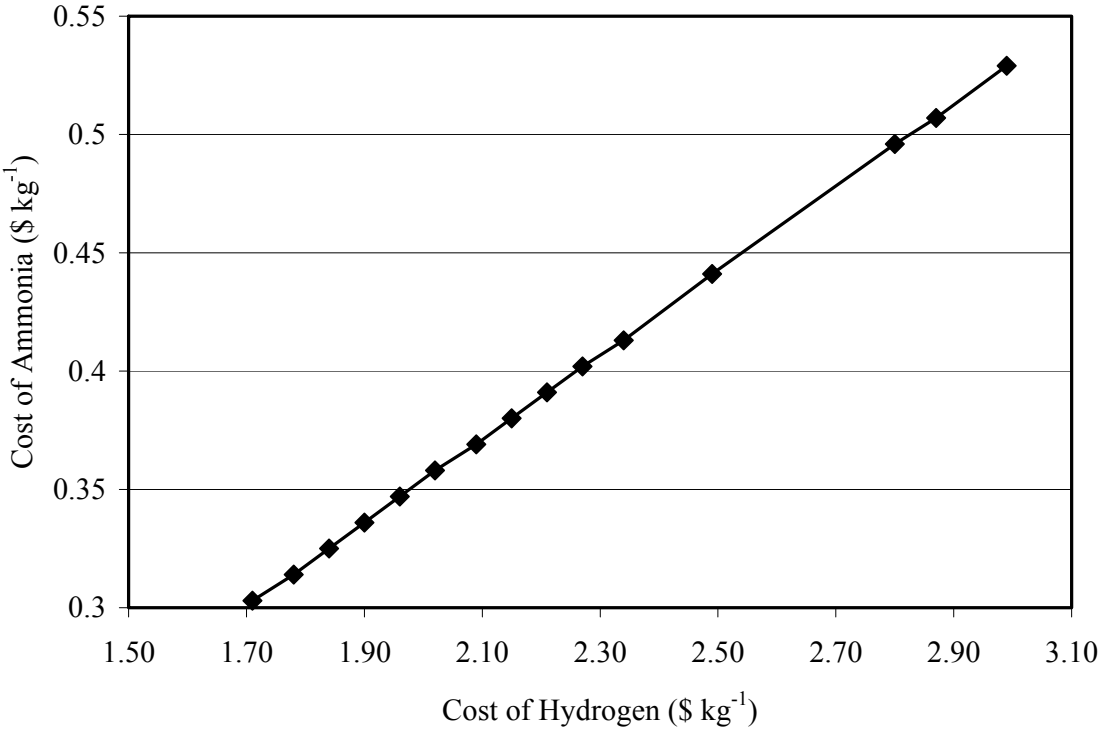

Figure 3.11: Sensitivity analysis on the effect of ammonia cost respective to the cost of hydrogen generated on board via ammonia electrolysis.

3.5 Conclusions

The electrolysis of ammonia was evaluated as a potential technology for the on-board storage and production of hydrogen. Carbon fiber paper was used as catalytic support and Ti foil used as the electrode shell and Ti gauze was used as the current collector. Both anode and cathode were prepared similarly and plated with a Pt-Ir alloy. The electrodes were tested in a sandwich-configured ammonia electrolytic cell (AEC) designed to reduce the ohmic resistance of the cell. A hydrophilic membrane was used to separate the pure gases. Hydrogen generated at the cathode was sent to a 4 W polymer electrolyte membrane fuel cell (PEMFC). Net electric energies were obtained

demonstrating the benefit of ammonia electrolysis as an on-board hydrogen storage system. According to scale-up calculations, using an *in situ* ammonia electrolyzer on board will allow a HFCV to travel 483 km between refueling by storing 203 L of aqueous ammonia. At $0.36 per kg of ammonia, the cost of producing hydrogen on board is $2.02 per kg.

Appendix A

Storage system costs, gravimetric, and volumetric capacities were calculated using a lightweight 60% peak energy-efficient HFCV that achieves a range of 483 km between refueling.

A.1. Fuel cell power requirement for ammonia HFCV

According to the DOE, a lightweight vehicle achieves 5.3 km L^{-1} and is 2.5 less efficient than a HFCV. A gallon of gasoline is equivalent (gge) to a kg of hydrogen.

$$ICE\ energy = 12.5\ gal \times 33.3\frac{kWh}{gal}$$

$$ICE\ energy = 416.25 kWh$$

$$Amount\ hydrogen = \frac{416.25 kWh}{2.5 \times 33\frac{kWh}{kg}} = 5 kg$$

In order to travel 483 km with a HFCV, 5 kg of hydrogen is required, which is echoed by the DOE [10]. On average, a car is refueled every 6 hours traveling 50 mph. The nominal fuel cell power required to move a lightweight HFCV is:

$$PEMFC\ power = \frac{416.25 kWh}{6h \times 2.5} = 27.75 kW$$

The fuel cell for our system has to be oversized since the ammonia electrolytic cell consumes 60% of the energy. This 60% increase in fuel cell cost, weight, and volume will be declared as part the storage system.

$$PEMFC\,required = \frac{27.75\,kW}{(1-60\%)} = 69.38\,kW$$

A.2. Storage system cost

The ammonia storage vessel, Teflon tubing, centrifugal pump, start-up hydrogen drum, compressor, and controller are common and commercially available equipment. These 6 items are estimated to cost $3,200. The AEC and PEMFC cost, weight, and volume are functions of several factors along with several assumptions, and their calculations are shown in detail.

With the increase in power required from the PEMFC comes an increase in the amount of hydrogen required between refueling.

$$Hydrogen = \frac{69.375\,kW \times 6h}{33\frac{kWh}{kg} \times 60\%} = 21.02\,kg$$

Faraday's Law can be used to predict the current required to produce 21.02 kg (3.5 kg h^{-1}) of hydrogen since ammonia electrolysis is 100% efficient.

$$Current = \frac{3{,}500\frac{kg}{h} \times 6\frac{e^-}{mol} \times 26.8\frac{Ah}{e^-}}{3 \times 2\frac{g}{mol}} = 93{,}800\,A$$

Current densities as high as 130 mA cm^{-2} with a cell potential of 0.45 V has been achieved at the EERL with 8.4 mg cm^{-2} Pt-Ir and is currently being improved. With this said, using electrodes with reactive geometric surface areas of 8.1 cm x 7.6 cm creates

electrodes with 61.94 cm^2 of surface area. In turn, 8 A can be applied per cell deducing that 11,725 cells are required to obtain 27.2 kW net energy for the motor.

The total catalyst required for the AEC (accounting for anode and cathode per cell):

$$Loading = 8.4\frac{mg}{cm^2} \times 2 \times 11{,}725 cells \times 61.94 cm^2 = 12.2 kg$$

Assuming that the cost of Ir is equivalent to the cost of Pt, which is expected to cost \$900 per troy ounce (\$2,646 per kg), can be determined. Due to the expense of noble metals, the AEC cost is completely dependent on the loading and catalyst costs meaning that the AEC cost can now be estimated.

$$AEC\,\mathrm{cost} = 12.2 kg \times \frac{\$2{,}646}{kg} = \$32{,}281$$

According to Fig. 3.9, 41.6 kW of the PEMFC are required for storage calculations. Using the \$35 per kW target the DOE has established for fuel cells:

$$PEMFC\,storage\,\mathrm{cost} = \frac{\$35}{kW} \times 41.6 kW = \$1{,}456$$

This brings the total system storage cost to \$36,937. In terms of the DOE technical storage targets which are summed up in Table 3.2:

$$Cost\,1 = \frac{\$36{,}937}{21.2 kg\, H_2} = \frac{\$1{,}742}{kg}$$

$$Cost\,2 = \frac{\$36{,}937}{33\frac{kWh}{kg} \times 60\% \times 21.2 kg} = \frac{\$88}{kWh}$$

A.3. Gravimetric capacity

The ammonia storage vessel, Teflon tubing, start-up drum, compressor, and process controller are estimated to weigh 26.5 kg based on commercially available products. The weight of fuel, storage part of the fuel cell, and AEC are calculated in detail.

$$NH_3\ fuel\ weight = 21.2\,kg\ H_2 \times \frac{1\,kg\ NH_3}{0.177\,kg\ H_2} = 119.8\,kg$$

According to Satyapal *et al*. [10], the target power density for PEMFCs is 2,000 W per kg. As a result, the storage part of the fuel cell will weigh 20.8 kg ($41.6\,kW \div 2\frac{kW}{kg}$). Using the assumption made earlier that the AEC is twice as heavy as the fuel cell, which is 69.4 kW.

$$AEC\ weight = \frac{2 \times 69.4\,kW}{2\frac{kW}{kg}} = 69.4\,kg$$

The total gravimetric capacity is determined using the total estimated storage system weight, which is 236.5 kg.

$$Gravimetric1 = \frac{21.2\,kg}{236.5\,kg} = 0.090$$

$$Gravimetric2 = \frac{21.2\,kg \times 33\frac{kWh}{kg} \times 60\%}{236.5\,kg} = 1.77\frac{kWh}{kg}$$

A.4. Volumetric capacity

Similarly, the volumes of the tubing, start-up drum, compressor, and process control are estimated to only occupy 97 L. Using the fact that 119.8 kg of ammonia is

required calculated in A.3. and a density of 682 kg m^{-3}, the storage vessel volume is 174 L. Again, the targeted power/volume density for PEMFCs is 2,000 W L^{-1} according to the DOE. Based on the 41.6 kW of fuel cell power that is used for storage, the storage part of the PEMFC requires 20.8 L. Using the 2 times relation for AEC:PEMFC for volume and weight, the AEC occupies:

$$AEC\,volume = \frac{2 \times 69.4\,kW}{2\frac{kW}{L}} = 69.4\,L$$

Total storage system volume required is 361.2 L. The volumetric storage parameters are as follows:

$$Volumetric1 = \frac{21.2\,kg}{361.2\,L} = 0.059\frac{kg}{L}$$

$$Volumetric2 = \frac{21.2\,kg \times 33\frac{kWh}{kg} \times 60\%}{361.2\,kg} = 1.16\frac{kWh}{L}$$

3.6 References

1. K. Weissermel, H.J. Arpe, Industrial Organic Chemistry. fourth ed., Wiley, Germany, 2003.
2. M. Granovskii, I. Dincer, M.A. Rosen, Environmental and economic aspects of hydrogen production and utilization in fuel cell vehicles, J. Power Sources. **157** (2006).
3. M. Granovskii, I. Dincer, M.A. Rosen, Exergetic life cycle assessment of hydrogen production from renewables, J. Power Sources. **167** (2007).
4. M.Z. Jacobson, W.G. Colella, D.M. Golden, Cleaning the air and improving health with hydrogen fuel-cell vehicles, Science. **308** (2005).
5. J.J. Hwang, D.Y. Wang, and N.C. Shih, Development of a lightweight fuel cell vehicle, J. Power Sources. **141** (2005).
6. M.W. Melaina, Initiating hydrogen infrastructures: preliminary analysis of a sufficient number of initial hydrogen stations in the US, Int. J. Hydrogen Energy, **38** (2003).
7. H.L. MacLean, L.B. Lave, Evaluating automobile fuel/propulsion system technologies. Progress in Energy and Combustion Science. **29** (2003) 1-69.
8. H.L. Maclean, L.B. Lave, Life cycle assessment of automobile/fuel options, Environ. Sci. Technol. **37** (2003).
9. M. Balat, N. Ozdemir, New and renewable hydrogen production processes, Energy Sources Part A. **27** (2005).
10. S. Satyapal, J. Petrovic, C. Read, G. Thomas, G. Ordaz, The US Department of Energy's National Hydrogen Storage Project: Progress towards meeting hydrogen-powered vehicle requirements, Catal. Today. **120** (2007).
11. G. Thomas, G. Parks, Potential roles of ammonia in a hydrogen economy: A study of issues related to the use of ammonia for on-board vehicular hydrogen storage, U.S. Department of Energy. (2006) 23.
12. F. Vitse, M. Cooper, G.G. Botte, On the use of ammonia electrolysis for hydrogen production, J. Power Sources. **142** (2005).
13. G.G. Botte, Carbon fiber-electrocatalysts for the Oxidation of Ammonia, Ethanol, and Coal, and their Application to Hydrogen Production, Fuel Cells, and Purification Processes. U.S. (2004) (patent pending).
14. G.G. Botte, F. Vitse, M. Cooper, Electrocatalysts for the Oxidation of Ammonia and their Application to Hydrogen Production, Fuel Cells, Sensors, and Purification Processes. U.S. (2003) (patent pending).
15. J. Laramine, A. Dicks, Fuel Cell Systems Explained, first ed., J.W. Sons, New York, 2003.
16. A.F. Bouwman, D.S Lee, W.A.H. Asman, F.J. Dentener, K.W. VanderHoek, J.G.J. Oliver, A global high-resolution emission inventory for ammonia, Global Biogeochem. Cycles, **11** (1997).
17. D.R. McCubbin, B.J. Apelberg, S. Roe, F.Divita, Livestock ammonia management and particulate-related health benefits, Environ. Sci. Technol. **36** (2002).

18. D.C. Bouchard, M.K. Williams, R.Y. Surampalli, Nitrate Contamination of Groundwater - Sources and Potential Health-Effectss, J. Am. Water Works Assn. **84** (1992).
19. S. Basakcilardan-Kabakci, A.N. Ipekoglu, I. Talini, Recovery of ammonia from human urine by stripping and absorption, Environ. Eng. Sci. **24** (2007).
20 .K.M. Udert, K.M., T.A. Larsen, W. Gujer, Estimating the precipitation potential in urine-collecting system, Water Res. **37** (2003).
21. A. Demirbas, Progress and recent trends in biofuels, Prog. Energy Combus. Sci. **33** (2007).
22. M. Cooper, G.G. Botte, Optimization of the electrodeposition of Raney nickel on titanium substrate, J. Mat. Sci. Lett. **41** (2006).
23. M. Cooper, G.G. Botte, Hydrogen production from the electro-oxidation of ammonia catalyzed by platinum and rhodium on raney nickel substrate, J. Electrochem. Soc. **153** (2006).
24. C.R.K. Rao, D.C. Trivedi, Chemical and electrochemical depositions of platinum group metals and their applications, Coord. Chem. Rev. **249** (2005).
25. F. Wu, H. Murakami, Y. Yamabe-Mitari, H. Harade, H. Katayama, Y. Yamamoto, Electrodeposition of Pt-Ir alloys on nickel-base single crystal superalloy TMS-75, Surf. Coat. Technol. **184** (2003).
26. D.J. Yang, J.X. Ma, L. Xu, M.Z. Wu, H.J. Wang, The effect of nitrogen oxides in air on the performance of proton exchange membrane fuel cell, Electrochim. Acta. **51** (2006).
27. G. Prentice, Electrochemical Engineering Principles. first ed., Prentice Hall, Saddle River, 1991.
28. E.J. Carlson, P. Kopf, J. Sinha, S. Sriramulu, Cost analysis of PEM Fuel Cell Systems for Transportation, NREL Subcontract Report SR-560-39104 (2005) 1-109.

CHAPTER 4.

UREA ELECTROLYSIS: DIRECT HYDROGEN PRODUCTION FROM URINE

It should be noted that the contents of this chapter are published in a peer-reviewed journal: B.K. Boggs, R.L. King, and G.G. Botte, *Chem. Commun.*, **2**, p. 4859-61 (2009).

4.1 Abstract

A new technology has been developed that accomplishes the direct conversion of urine and urea to pure hydrogen via electrochemical oxidation with an inexpensive nickel catalyst.

4.2 Introduction

The utilization of wastewater for useful fuel has been gathering recent attention due to society's need for alternative energy sources. The electrooxidation of urea found at high concentrations in wastewater simultaneously accomplishes fuel production and remediation of harmful nitrogen compounds that currently make their way into the atmosphere and groundwater. Pure hydrogen was collected in the cathode compartment at 1.4 V cell potential, where water electrolysis does not occur appreciably. It was determined that an inexpensive nickel catalyst is the most active and stable for the process. Urine is the most abundant waste on Earth. The largest constituent of urine is urea, which is a significant organic source of H, C, O, and N. Despite the numerous benefits of using urea/urine for hydrogen production [1], there is not a single technology that directly converts urea to

hydrogen [1,2]. In addition to sustaining hydrogen resources, such a process could denitrificate urea-rich water that is commonly purged into rivers, creeks, and tributaries from municipal wastewater treatment plants. Currently, nitrate concentration in these waters is regulated at 10 mg L^{-1}, but available denitrification technologies are expensive and inefficient [3]. Converting urea to valuable products before it naturally hydrolyzes to ammonia, which generates gas-phase ammonia emissions and contributes to ammonium sulfate and nitrate formation in the atmosphere, will save billions of dollars spent each year on health costs [4]. Here we demonstrate a technology for improving hydrogen resources for energy sustainability by recycling waste materials such as human excreta. We have developed an electrochemical process that produces H_2 from urine/urea as shown in figure 4.1 [5].

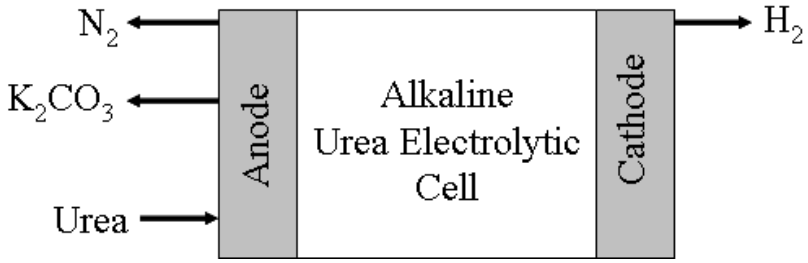

Figure 4.1: Schematic representation of the direct urea-to-hydrogen process

Our results demonstrate that human urine, with an average concentration of 0.33 M urea [6], can be electrochemically oxidized with an inexpensive transition metal, nickel, according to Eqns. 1-4.

$$CO(NH_2)_{2(aq)} + 6OH^- \rightarrow N_{2(g)} + 5H_2O_{(l)} + CO_{2(aq)} + 6e^- \quad (1)$$

$$Ni(OH)_{2(s)} + OH^- \rightarrow NiOOH_{(s)} + H_2O_{(l)} + e^- \quad (2)$$

$$6\,H_2O_{(l)} + 6\,e^- \rightarrow 3\,H_{2(g)} + 6\,OH^- \quad (3)$$

$$CO(NH_2)_{2(aq)} + H_2O_{(l)} \rightarrow N_{2(g)} + 3H_{2(g)} + CO_{2(aq)} \quad (4)$$

Urea is oxidized at the anode (Eqn. 1) at a standard electrode potential of -0.034 V/SHE. The oxidation of $Ni(OH)_2$ to NiOOH at the anode (Eqn. 2) is a competing reaction that attributes to current during electrolysis and occurs at 0.49 V/SHE. Alkaline reduction of water (Eqn. 3) occurs on the cathode at -0.83 V/SHE. Overall in Eqn. 4, a cell potential of only 0.865 V is thermodynamically required to electrolyze urea at standard conditions. This is significantly less than the 1.23 V required to electrolyze water theoretically generating 30% cheaper hydrogen. Nitrogen is generated from the anode demonstrating nitrate remediation of wastewater while water is reduced at the cathode producing valuable hydrogen for the impending hydrogen economy.

4.3 Results and discussion

Figure 4.2a shows the cyclic voltammogram (CV) comparison of different electrocatalysts (Pt, Pt-Ir, Rh, and Ni) for the electrooxidation of urea in alkaline media. Polarization curves between the various metals in the presence and absence of 0.33 M urea and 5 M KOH at a scan rate of 10 mV s^{-1} from -0.1 to 0.8 V versus Hg/HgO reference supported by a Luggin capillary at 25ºC shows that Ni is the most active catalyst in terms of current density. The electrodes were 4 cm^2 based on geometric area of Ti foil (inert) deposited with an average 10.0 ± 0.1 mg of respective

metal. The counter electrode was a 25 cm^2 Pt foil. All electrochemical experiments were performed in a conventional three-electrode cell powered by a Solartron 1281 Multiplexer potentiostat. Figure 4.2b, constant voltage analysis at 1.4 V in 5 M KOH/0.33 M urea at 25ºC, further shows Ni is the most stable and active electrocatalyst for the electrooxidation of urea in alkaline media. This potential was chosen from the fact that water reduction is kinetically friendly at -0.83 V/SHE [7-9] (standard hydrogen electrode), and the electrooxidation of urea is occurring at 0.55 V vs. Hg/HgO according to Figure 4.2c. Nickel in basic media is rapidly converted to $Ni(OH)_2$ which is further oxidized to NiOOH. This $Ni^{2+/}Ni^{3+}$ redox reaction enhances catalytic electrooxidation behavior of small organic compounds [9-11]. The oxidation of $Ni(OH)_2$ to NiOOH is represented by anodic peak a_1. Figure 2c shows that urea electrolysis begins at the same potential where NiOOH is formed, suggesting that Ni^{3+} is the active form for urea oxidation. This is seen as an increase of current density at a_1 in the presence of urea. Furthermore, a change in slope due to the onset of water electrolysis can be seen at more positive potentials.

We found that nickel oxyhydroxide modified nickel electrodes (NOMN) for urea electrooxidation on different metallic substrates (Ni foil, Ni gauze, Ti foil, and Ti gauze) that have been electroplated with 10.0 ± 0.1 mg of Ni using a Watts bath then activated following the procedure developed by Vaze, Sawant, and Pangarkar [10] yield higher current densities than those of M/Ni, where M represents the metallic substrate.

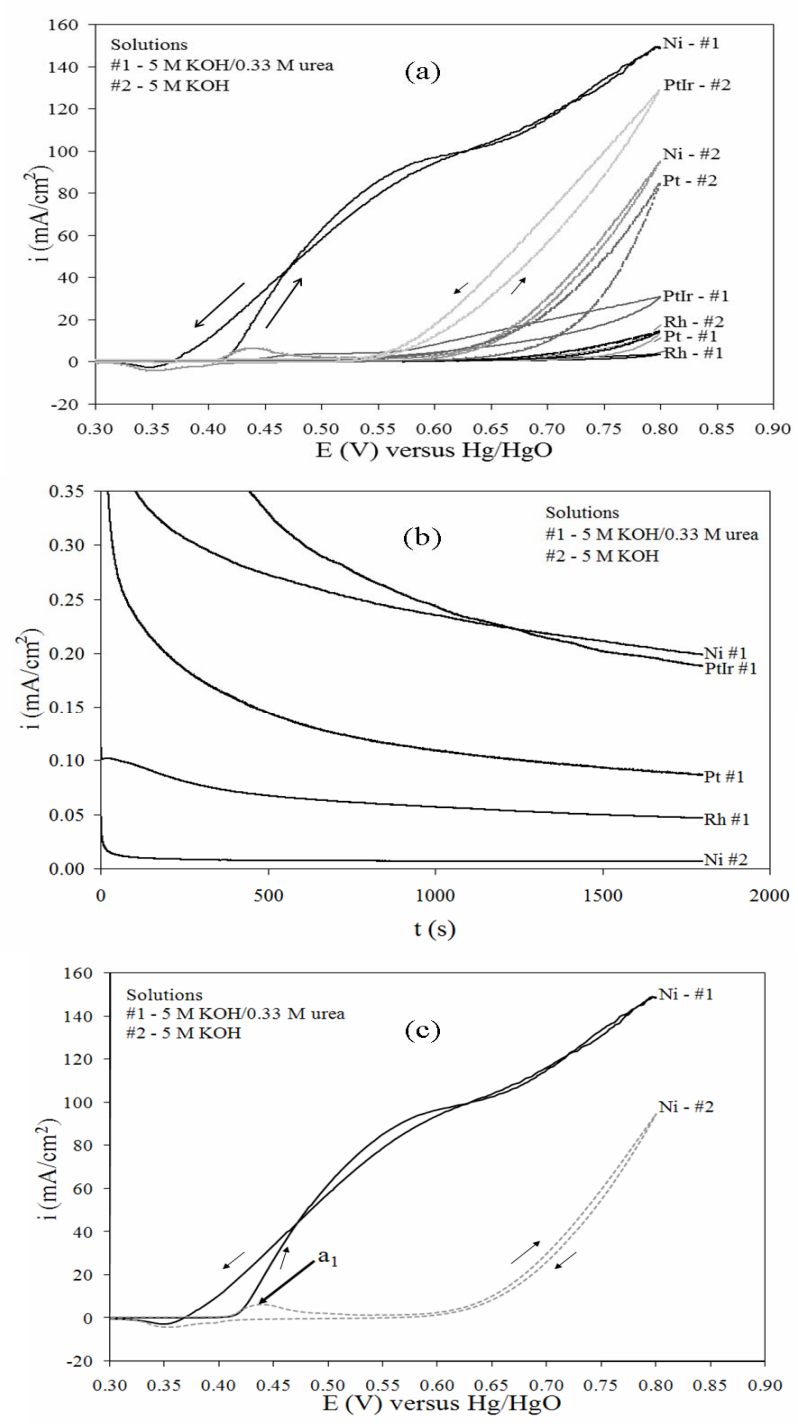

Figure 4.2: Anode catalyst analysis at 25ºC (a) cyclic voltammograms obtained in 5 M KOH with and without the presence of urea on Ti-foil supported electrodes with a 10 mV s^{-1} scan; (b) constant voltage test with 1.4 V potential step with 5 M KOH/0.33 M urea; (c) cyclic voltammogram of Ni/Ti electrode in the absence (grey) and presence (black) of 0.33 M KOH in 5 M KOH solution.

NOMN electrodes were used for the remaining electrochemical behavior analyses. Figure 4.3 demonstrates that there is an influence of scan rate on the cyclic voltammetry behavior of NOMN electrodes. The electrooxidation of urea in this system was characterized with CVs from 0.0 to 0.6 V versus Hg/HgO at scan rates of 5 to 95 mV s^{-1}. Figure 4.3a shows that the cathodic peak does not shift in potential as the scan rate increases in the presence of urea. The curves are shown from 0.0 to 0.5 V for scaling purposes. Figure 4.3b indicates that cyclic voltammetry peak cathodic currents (I_{pc}) followed a linear correlation with the square root of the scan rate (R^2= 0.976). Together, these criteria confirm that the production of NiOOH from $Ni(OH)_2$ is a reversible diffusion-controlled process. The increase in cathodic currents as a function of scan rate indicates that the electrooxidation of urea is slower than the electrooxidation of nickel species to a higher valence state. Therefore, we hypothesize that the catalytic oxidation of urea is slow and the rate-limiting step is the reaction between Ni^{3+} and urea absorbed on the surface.

The electrocatalytic behavior of the NOMN electrode towards urea oxidation in basic media was further studied with cyclic voltammetry and constant voltage analyses at varying operating conditions. It was found that the current density increases with temperature. Also, higher concentrations of KOH favor the reaction rate. As the concentration of KOH exceeded 5 M, the NOMN electrode lost activity as seen by a decrease in current density during constant voltage analyses. This could be due to faster disappearance of the oxide layer, which was visibly evident.

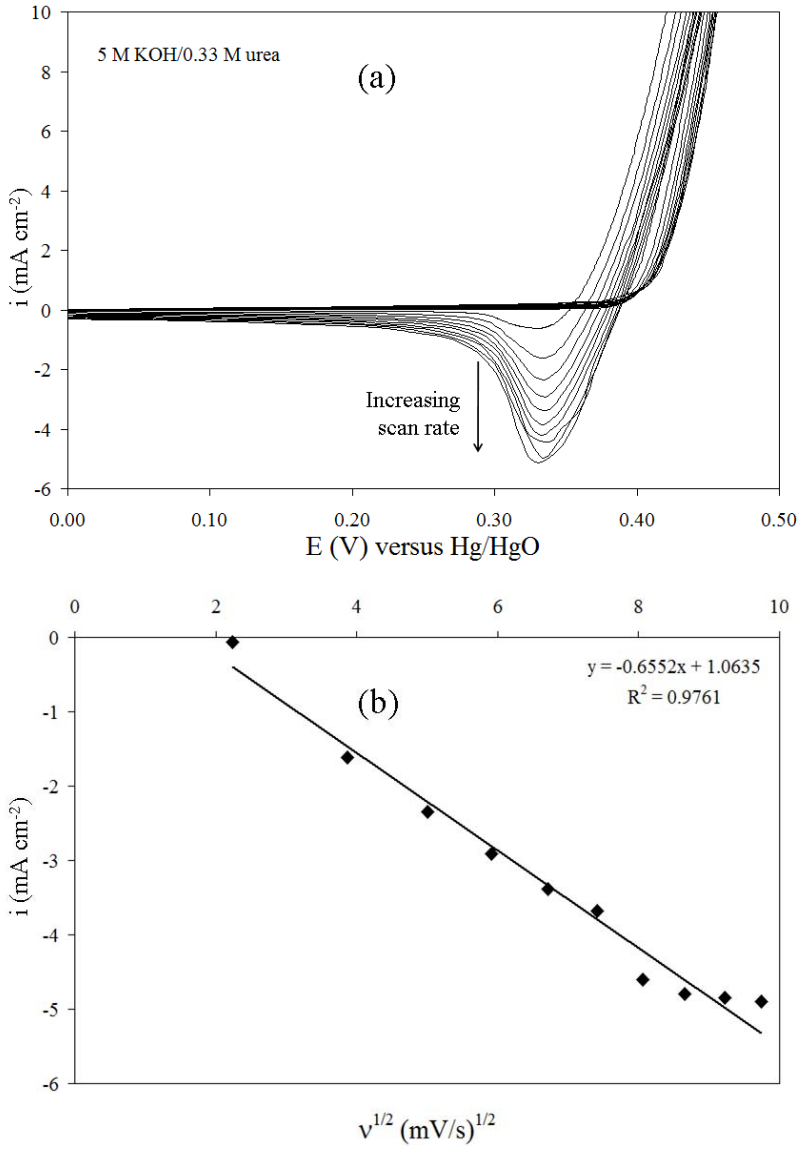

Figure 4.3: (a) Cyclic voltammograms obtained in 5 M KOH + 0.33 M urea for the NOMN electrode with various scan rates (ν) from 5 mV s^{-1} to 95 mV s^{-1}. (b) the plot of cathodic current density variation with $\nu^{1/2}$.

Energy dispersive X-ray (EDX) microanalyses of a Ti foil (99.99% pure) electrode (deposited with 10.0 ± 0.1 mg of Ni and then activated into a NOMN electrode) before and after urea electrolysis at 1.4 V for 30 minutes in 5 M KOH/0.33

M urea shows that the amount of atomic carbon and oxygen on the electrode surface increases during electrolysis. This may be contributed to adsorption of products onto the surface. As a result, the surface atomic composition of Ni decreases leading to decay in the current density during the constant voltage study.

Anode and cathode gases were collected separately in a Hoffman apparatus filled with a solution of 5 M KOH in the presence and absence of 0.33 M urea and analyzed via gas chromatography. The electrolysis were performed at a constant voltage of 1.5 V and 25ºC for 22 hours. Currents observed were 20 mA and less than 1 mA in the presence and absence of urea, respectively. This verifies that water electrolysis is not occurring to an appreciable extent. Pure H_2 was observed at the cathode while N_2 (96.1%) with trace amounts of O_2 (1.9%) and H_2 (2.0%) were detected at the anode for urea electrolysis. A small amount of hydrogen (0.28%) was detected at the anode in the absence of urea as well, which suggests this hydrogen is not a product of urea electrolysis. Instead, it is likely due to the nickel transition reaction $Ni(OH)_2 \rightarrow NiOOH$. Carbon dioxide was not detected as part of the gas phase for urea electrolysis, but is believed to have formed potassium carbonate in the liquid phase. After 22 electrolysis hours, 13% of the urea was converted into hydrogen, nitrogen, and potassium carbonate, as determined using a heat treatment method for urea determination.

We have demonstrated that urea/urine can be used for the production of H_2 through this new technology utilizing inexpensive Ni. This is further demonstrated via cyclic voltammetry shown Figure 4.4. Theoretically, hydrogen can be produced at

$1.62 kg^{-1} based on an electricity cost of $0.07 kWh^{-1} and the proposed electrochemical reactions (Eqns. 1-4) that have been developed from electrochemical data and gas analyses.

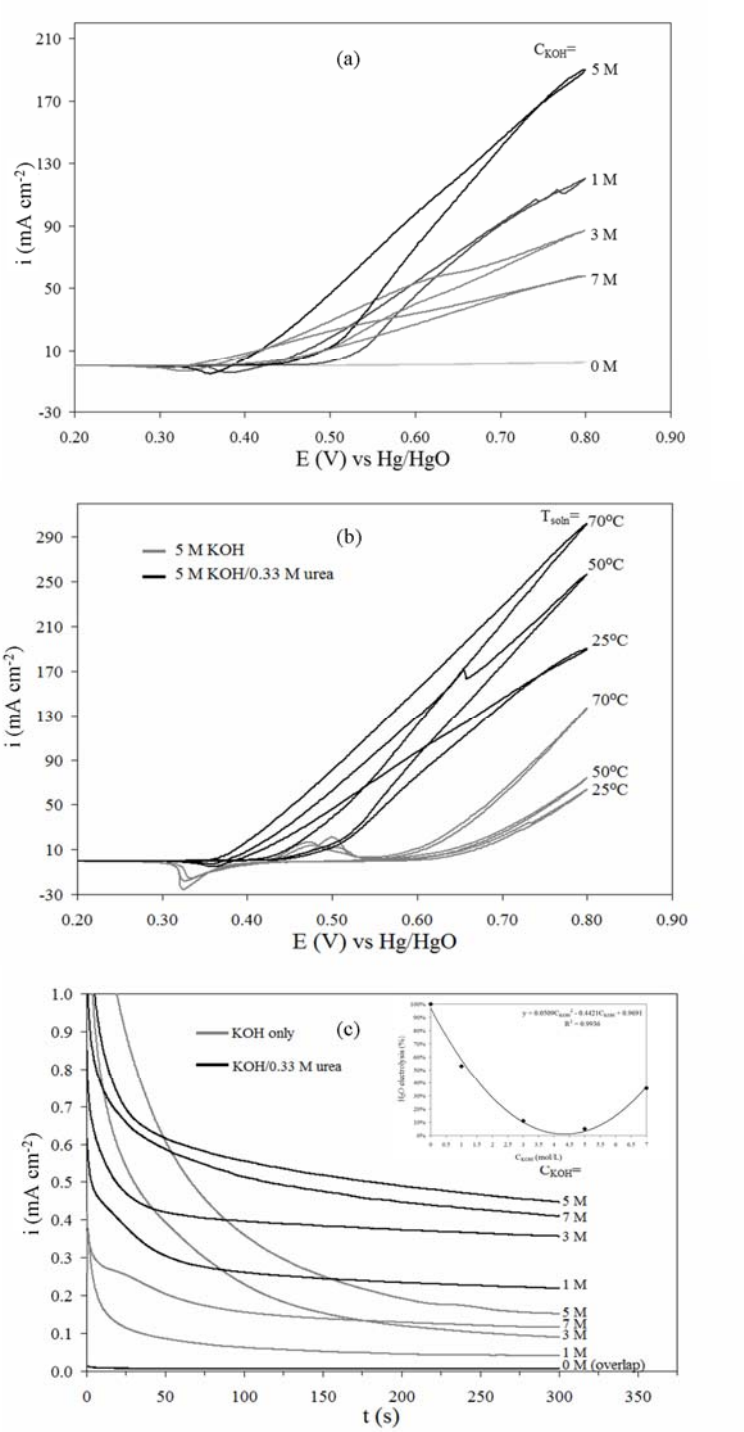

Figure 4.4: Operating conditions effects on electrooxidation of urea. Effect of (a) KOH concentration on CV behavior, (b) Temperature on CV behavior, and (c) KOH concentration on potentiostatic performance.

Table 4.1 shows energy consumption (Wh per gram of hydrogen) and cost of hydrogen comparison between urea and water electrolysis at standard conditions with Ni anodes. We found that 34% less energy is required for urea electrolysis, which generated 36% cheaper hydrogen compared to water electrolysis.

Table 4.1: Energy and hydrogen cost comparison between urea and water electrolysis based on an energy cost of \$0.07 kWh^{-1}

Electrolysis	*Energy* ($Wh\ g^{-1}$)	*H_2 Cost* ($\$\ kg^{-1}$)
Urea	37.5	2.63
Water	53.6	4.13

In the past, research pertaining to urea electrolysis exclusively involved the possibility of developing artificial kidneys for portable dialysis devices utilizing platinum electrodes in acidic buffers [12-15]. There is great interest in the scientific community for finding non-platinized catalyst alternatives such as Ni for hydrogen production. We have demonstrated that the technology is effective for both urea and urine.

4.4 Experimental/materials and methods

4.4.1 Electrode preparation

All chemicals and supplies were high purity (> 99.9%) and supplied from Alfa Aesar or Fisher Scientific. For anodic catalyst selection, 5 cm^2 titanium foil (0.127 mm thick) was used for working electrode substrates. Nickel foil (5 cm^2 0.127 mm thick) was used for nickel oxyhydroxide modified nickel electrode (NOMN) substrates. Titanium wire (0.25 mm diameter) was connected to the working electrode substrates by cutting a

small 1 mm slit in the foils and penetrating the Ti wire through the electrode. Pliers and a hand press were used to secure the connection. After constructing the anodes, the electrodes were rinsed with acetone and HPLC-grade ultrapure water. They were dried in an oven, and the electrode weights were recorded in order to determine catalyst loadings. Platinum foil counter (25 cm^2) was used for both electroplating and testing the anodes. The Pt-foil cathode was constructed similarly to the anodes.

4.4.2 Catalyst deposition

Table 4.2 shows catalyst plating conditions. The concentration of each metal in the bath was 160 mg L^{-1}. All of the salts were 99.99% pure from Alfa Aesar. Deposition potentials were experimentally determined using cyclic voltammetry using the setup in Figure 4.5. All electrodes in this study were plated potentiostatically with this same setup. A 2.5 cm stir bar at 60 rpm kept the bath solutions mixed during experimentation minimizing concentration gradients.

Table 4.2: Electrocatalyst plating conditions

Metal	Anode (foil)	Electrolyte	Salts	Temperature (ºC)	Plating Potential (V versus Ag/AgCl)
Rh	Pt	1 M HCl/HPLC	$RhCl_3 \cdot 3H_2O$	78	-0.12
Pt	Pt	1 M HCl/HPLC	$H_2PtCl_6 \cdot 6H_2O$	78	-0.12
Pt-Ir	Pt	1 M HCl/HPLC	$H_2PtCl_6 \cdot 6H_2O$ + $IrCl_3 \cdot 3H_2O$	78	-0.12
Ni	Ni	0.5 M $B(OH)_3$/HPLC	$NiSO_4 \cdot 7H_2O$ + $NiCl_2 \cdot 6H_2O$	45	-0.80

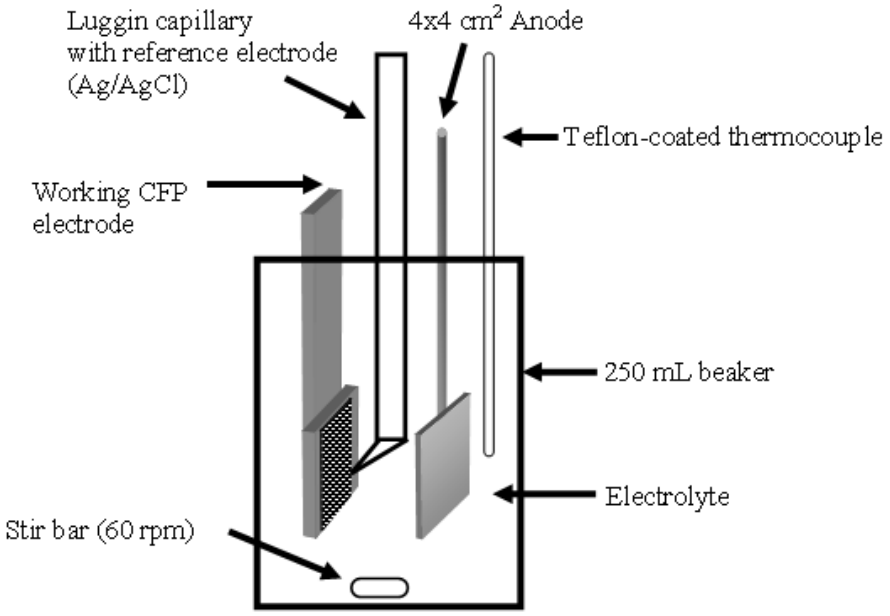

Figure 4.5: Plating setup. A Luggin capillary was used for cyclic voltammetry plating potential determination and was removed for electrodeposition.

Koslow Scientific supplied the Ag/AgCl reference electrode (+0.2224 V versus SHE) supported by a home-made Luggin capillary filled with its respective electrolyte. The tip of the Luggin capillary was placed 1 mm from the center of the working electrode. Platinum foil (0.01 cm thick, 99.999% pure from ESPI Metals) acted as the anode for plating except in the case of Ni, which utilized Ni foil (0.127 mm thick). The Ni electrode was plated using the common Watts bath. All of the plating solutions prepared here were solvated with ultrapure high performance liquid chromatography (HPLC) water.

4.4.3 Activation

A variety of procedures can be employed to activate a nickel electrode to the NOMN form [17-19]. The activation solution used here consisted of nickel sulfate (0.05 M), sodium acetate (0.10 M) and sodium hydroxide (0.005 M)). The activation was affected by holding the nickel electrode at 6.25 A m^{-2} galvanostatically with a stainless steel counter electrode at 33˚C. Polarity switching was employed such that the nickel electrode was used as the anode and cathode twice each for one minute. The same nickel electrode was then held as the anode and cathode for two minutes each, before two hours of further activation with the nickel kept as the anode.

4.4.4 Gas chromatography

The gaseous products at each electrode were collected separately using a Hoffman electrolysis apparatus (Fisher Scientific) filled with 0.33 M urea and 5 M KOH. A

potential of 1.5 V was applied with an Arbin BT2000 potentiostat for 22 hours to allow for sufficient gas production. The anode was a 20 cm^2 Ni foil (99.99% pure) that was deposited with 34.0 ± 0.1 mg of Ni and activated to form a NOMN electrode. The cathode was a 25 cm^2 Pt foil (99.999% pure). A 10 mL gas sample was extracted from each column and injected into the GC (SRI 8610 multi-gas) sample loop to ensure removal of any residual gases. Finally, 0.1 mL from the sample loop was then injected onto Haysep and mol sieve columns with a TCD detector.

4.4.5 Urea determination

Six urea standards of different concentrations were prepared in the range of 0.10 to 0.33 M urea in 7 M KOH. The solutions were sealed in 250 mL brown plastic bottles and heated at 70˚C for 22 hours. The bottles were then allowed to cool to room temperature for 5.5 hours. Each bottle was then opened and allowed to equilibrate with air for exactly one minute before extracting 1 mL with a volumetric pipette and diluting to 100 mL. A 45 mL aliquot of each diluted solution was treated with 1 mL pH adjusting solution and tested with an ammonia ISE (Ion-selective electrode, Orion 9512 Ammonia Electrode) for determination of ammonia concentration in ppm. These results were compiled to create a calibration curve for urea determination (Figure 4.6). An exponential curve fits the data points with R^2 value of 0.9966, meaning that 99.7% of the variation in NH_3 concentration can be explained by the variation in urea concentration with the exponential relationship.

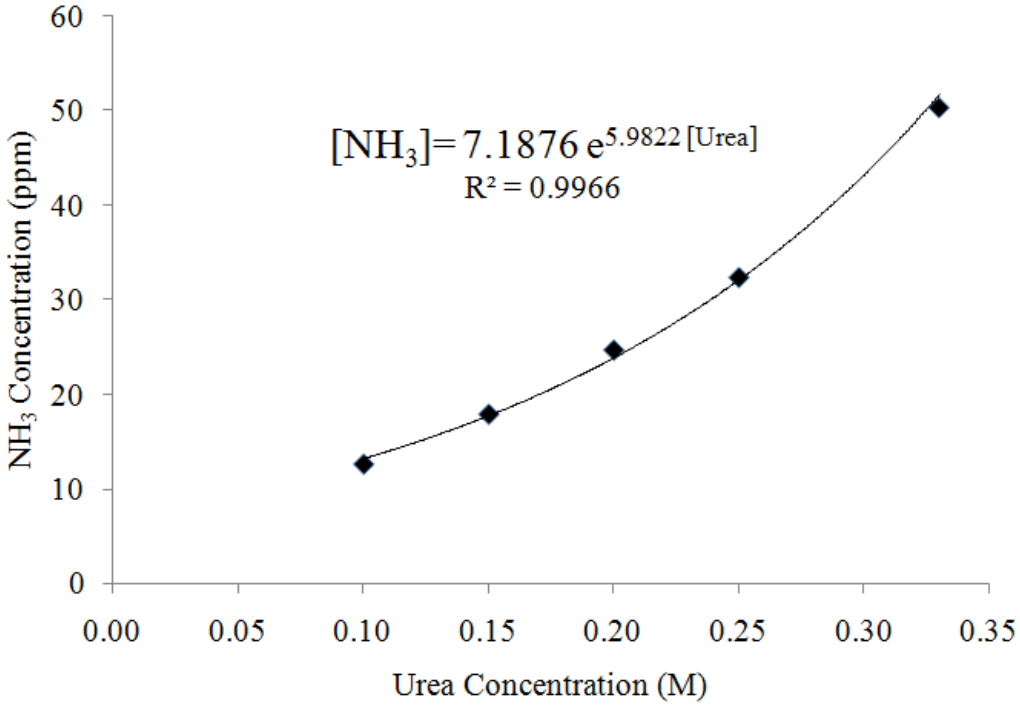

Figure 4.6: Calibration Curve for determination of urea concentration

4.5 Urine versus urea

In order to demonstrate that the oxidation of urea is similar to that of human urine, a cyclic voltammetry comparison was made using 3 different electrolytes. First, a baseline comparison in 1 M KOH was made followed by a solution of 1 M KOH with 0.33 M urea. Finally, a solution consisting of 1 M KOH and human urine was tested and compared. The anode was 2 cm x 2 cm 100-mesh Ni gauze that was sandblasted with a 2 cm x 2.5 cm 0.4 mg cm^{-2} Pt on carbon paper cathode. The CV was conducted at room temperature with a 10 mV s^{-1} sweep rate from 0 to 0.8 V versus Hg/HgO reference electrode. It can be concluded that human urine oxidizes similarly, with a higher current density, to a solution of synthetic urine composed of urea.

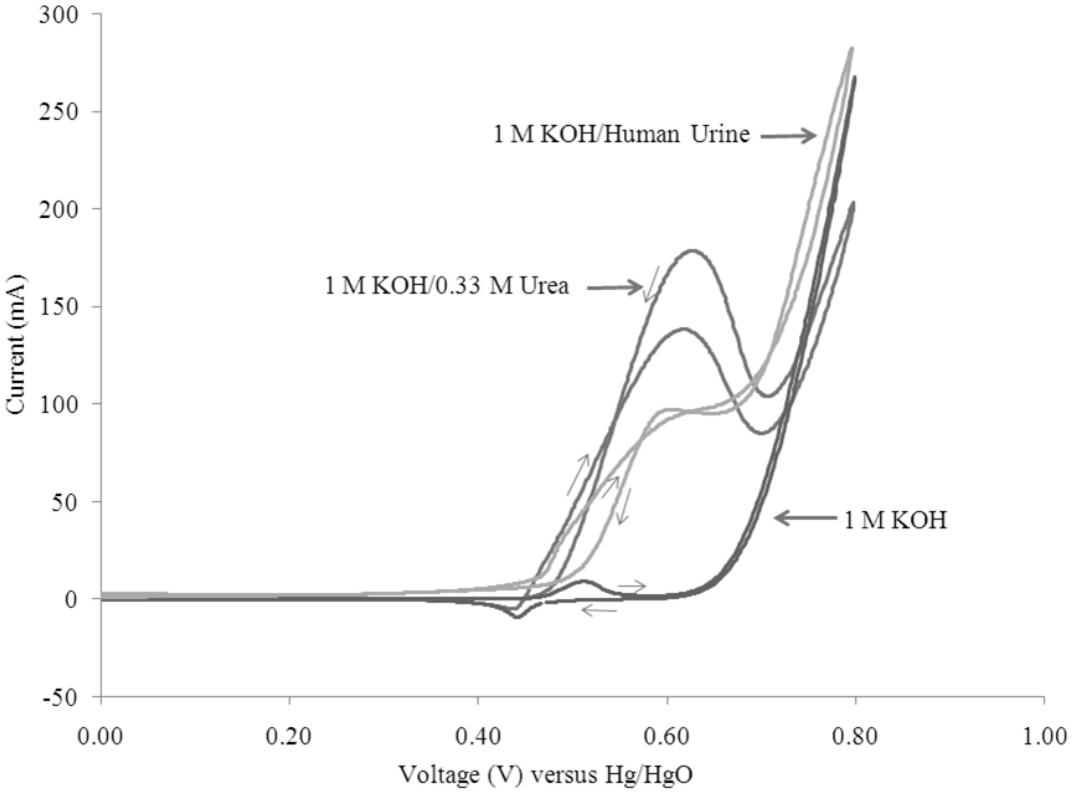

Figure 4.7: Cyclic voltammogram comparison of oxidation of synthetic urine (as urea) to that of human urine.

4.6 References

1. Research on Applied Bioelectrochemistry, Quarterly Progress Report No. 2, Magna Corporation Contract NASw-623, 1963.
2. H. B. H. Cooper, I. Spencer and W. Herbert, Methods for the production of ammonia from urea and/or biuret, and uses for NOx and/or particulate matter removal, U.S. Pat., 6 077 491, 2000.
3. D. C. Bouchard, M. K. Williams and R. Y. Surampalli, J. Am. Water Works Assoc., **84** (1992).
4. D. R. McCubbin, B. J. Apelberg, S. Roe and F. Divita, Environ. Sci. Technol., **36** (2002).
5. G. G. Botte, Electrolysis of urea/urine to produce ammonia and hydrogen, electrolysis of urea/urine to ammonia, and methods, uses, and fuel cells related thereto, U.S. Pat., 60/980 056, 2007.
6. Urine, Britannica Online Encyclopedia, http://www.britannica.com/EBchecked/topic/619857/urine, 2007.
7. F. Vitse, M. Cooper and G. G. Botte, J. Power Sources, **142** (2005).
8. G. G. Botte, F. Vitse and M. Cooper, Electrocatalysts for the oxidation of ammonia and their application to hydrogen production, fuel cells, sensors, and purification processes, U.S. Pat., 7 485 211 2003.
9. Q. Yi, W. Huang, J. Zhang, X. Liu and L. Li, J. Electroanal. Chem., **610** (2007).
10. A. S. Vaze, S. B. Sawant and V. G. Pangarkar, J. Appl. Electrochem., **27** (1997).
11. H. J. Schafer, Top. Curr. Chem., **142** (1987).
12. A. E. Bolzan and T. Iwasita, Electrochim. Acta, **33** (1988).
13. V. Climent, A. Rodes, J. M. Ort, A. Aldaz and J. M. Feliu, J. Electroanal. Chem., **461** (1999).
14. F. C. Nart and T. Iwasita, Electrochim. Acta, **37** (1992).
15. S. J. Yao, K. S. Walfson, B. K. Ahn and C. C. Liu, Nature, **241** (1973).

CHAPTER 5.

CONCLUSIONS AND RECOMMENDATIONS

5.1 Conclusions

5.1.1 Ammonia electrolysis in alkaline media: electrocatalyst optimization

It was shown that Pt-Ir on carbon fiber paper electrodes is the most active electrocatalyst in terms of maximizing the oxidation of ammonia with the least overpotential. In terms of minimizing the ammonia oxidation overpotential, catalyst selection is ranked as follows Pt-Ir-Rh >Pt-Ru > Pt-Rh > Pt-Ir > Ru > Ni > Pt > Rh. With regards to maximizing the exchange current density, the ranking is Pt-Ir > Pt-Rh > Pt > Pt-Ir-Rh > Pt-Ru > Rh > Ni > Ru. Due to the large exchange current density and average oxidation overpotential, Pt-Ir was chosen as the most active and suitable electrocatalyst to further optimize.

After determining that Pt-Ir is the most suitable catalyst for ammonia oxidation, the electroplating bath was optimized. It was found that the concentrations of Pt (IV) and Ir (III) in the deposition bath significantly alter the deposition behavior of the alloy and the electrochemical behavior. It was found through the use of statistical software, that a bath of consisting of 8.84 g L^{-1} Pt (IV) and 4.11 g L^{-1} Ir (III) was optimal for maximizing oxidation exchange current densities and minimizing oxidation overpotentials. With these same goals in mind, the optimal catalytic loading of Pt-Ir was 5.50 mg cm^{-2} based on geometric surface area.

5.1.2 Ammonia as an on-board hydrogen storage system

On-board hydrogen storage and production via ammonia electrolysis was evaluated to determine whether the process was feasible using galvanostatic studies between an ammonia electrolytic cell (AEC) and a breathable proton exchange membrane fuel cell (PEMFC). Hydrogen-dense liquid ammonia stored at ambient temperature and pressure is an excellent source for hydrogen storage. This hydrogen is released from ammonia through electrolysis, which theoretically consumes 95% less energy than water electrolysis; 1.55 Wh per gram of H_2 is required for ammonia electrolysis and 33 Wh per gram of H_2 for water electrolysis. An ammonia electrolytic cell (AEC), comprised of carbon fiber paper (CFP) electrodes supported by Ti foil and deposited with Pt-Ir, was designed and constructed for electrolyzing an alkaline ammonia solution. Hydrogen from the cathode compartment of the AEC was fed to a polymer exchange membrane fuel cell (PEMFC). In terms of electric energy, input to the AEC was less than the output from the PEMFC yielding net electrical energies as high as 9.7 ± 1.1 Wh g^{-1} H_2 while maintaining H_2 production equivalent to consumption.

Figure 5.1a shows a progression of the self-sustaining mobile application. Prototype I was an initial hypothesis testing as to whether or not the technology is feasible for mobile applications such as a shoe-sized automobile. A battery pack consisting of one AA battery powered the ammonia electrolysis in the Erlenmeyer flask. Both nitrogen and hydrogen generated in the flask were sent directly to the air-breathable PEMFC. A DC-geared motor was connected to the PEMFC. This concept worked relatively well, however ammonia fumes were carried into the fuel cell which is highly

detrimental. To solve this issue, Prototype II was created. The gases were sent to an HCl scrubber to prevent any ammonia fume carry over to the fuel cell. This worked, but the system still required more energy input than what was being produced. Prototype III replaced the carbon-fiber wrapped electrodes in Prototypes I and II with optimized Pt-Ir electrodes on carbon-fiber paper. This optimization is discussed in Chapter 1. In addition, a new cell design described in Chapter 3 was used for the AEC. Separating the gases made the overall system more efficient allowing the system to become self sufficient until ammonia was depleted. The battery pack would be used only for starting the system until steady state was reached. A similar stationary application taken from Prototype III was created further demonstrating the potential of ammonia electrolysis as an alternative energy source.

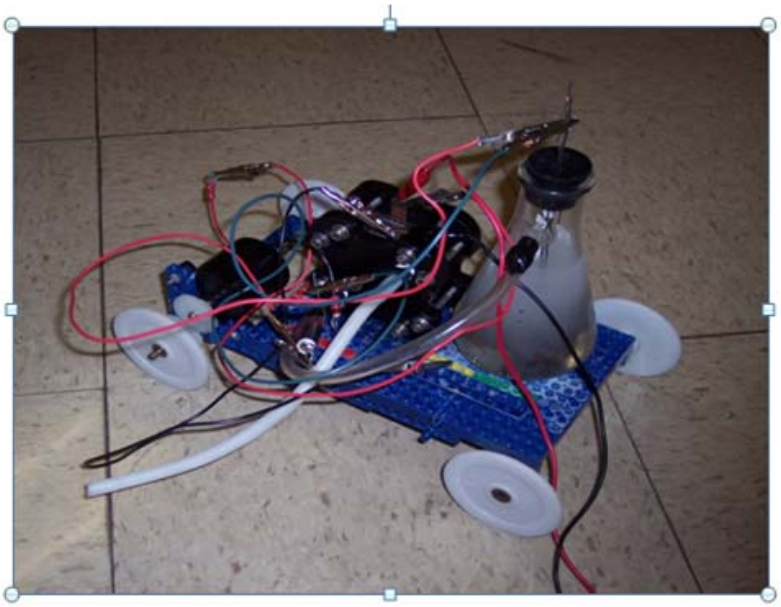

Prototype I

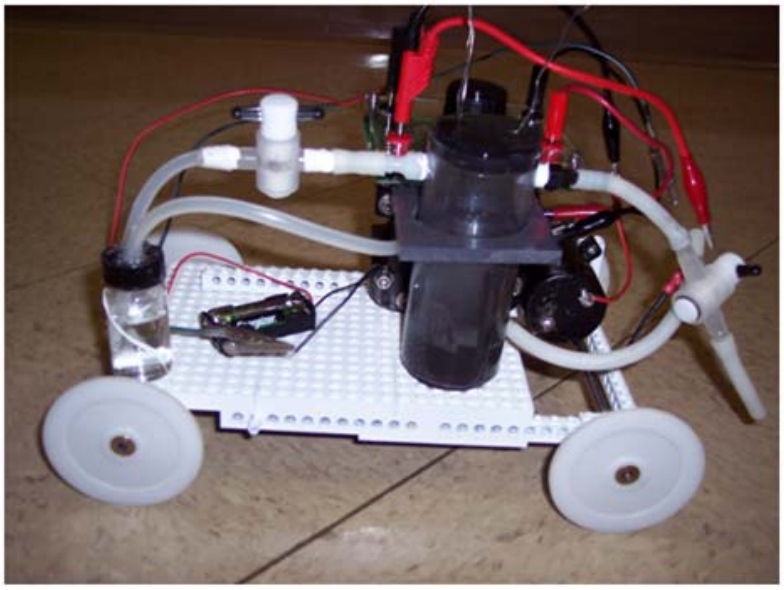

Prototype II

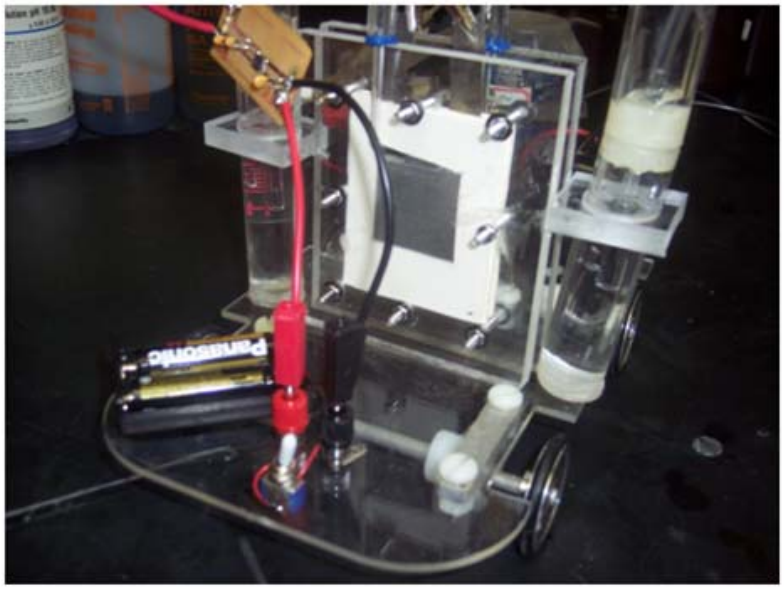

Prototype III

Figure 5.1: Evolution of mobile and stationary applications using in situ ammonia electrolysis in alkaline media

5.1.3 Urea electrolysis in alkaline media

This novel technology directly converts urine into hydrogen while mitigating nitrate contamination in ground and drinking water. The conception of this technology is shown here which encompasses understanding the electrochemical behavior through the use of in-situ and ex-situ experiments as well as finding an optimum catalyst for urea oxidation in alkaline media.

It was found that inexpensive Ni is the most active electrocatalyst for the oxidation of urea. Coupled with similar Ni electrodes used for alkaline water reduction in the chloralkali industry, alkaline urea electrolysis offers an economic, environmental, and feasible method for mass hydrogen production.

5.2 Recommendations

5.2.1 Ammonia electrolysis in alkaline media: electrode design

The electrode design discussed in Chapters 2 and 3 offered the lowest energy consumption for ammonia electrolysis in alkaline media as shown in open literature. Minimizing ohmic losses by reducing electrical resistance was a major focus of research that allowed for the results presented here. However, it is believed that these electroplated CFP electrodes can be improved by:

- Pretreating the Ti current collectors with a strong acid such as aqua regia in an effort to remove any highly electrically resistant layers of titanium oxide.
- Coating these pretreated Ti current collectors with a more conductive metal, such as Ni, either electrochemically or by way of other common coating technologies.

- Synthesizing the Pt-Ir catalyst on the CFP using a similar technique that the fuel cell industry uses will increase electrokinetics and reduce energy consumption.

5.2.2 Ammonia electrolysis in alkaline media: cell design

All of the results presented here were using worst case conditions. Making the AEC dynamic rather than static will improve concentration gradients and overall performance. Similarly, designing a cell that can be heated to temperatures of 60-70°C will drastically reduce energy consumption. This behavior was observed in beaker analyses. In addition, it is necessary to break down resistances in the cell which are contributing to voltage drops. For instance, solution and membrane resistance can have a significant effect on overall cell performance as well as the electrode distances from the membrane.

5.2.3 Urea electrolysis in alkaline media: electrode design

Chapter 4 presented the birth of alkaline urea electrolysis. Simple Ti mesh electrodes that were sandblasted then coated with their respective metal electrochemically were used. These electrodes allowed for accurate and inert conditions for characterizing different metals. Electrodes that offer higher electrochemically active surface area are still required to be designed.

5.2.4 Urea electrolysis in alkaline media: electrocatalysts

Common electrocatalysts for oxidizing small organic compounds were investigated and compared. More tests of different binary and ternary combinations of these metals are necessary.